UNIVERSITAT POLITECNICA
DE VALENCIA

School of Engineering in Geodesy, Cartography
and Surveying

# Documentation of Cultural Heritage using 3D Laser Scanning and Close-Range Photogrammetry


Author:
Paola Avila Forero

Supervisor:
Dra. Matilde Balaguer Puig

Valencia, September 2019

*"Our rich and varied cultural heritage has a profound power to help build our nation"*

Nelson Mandela

## Acknowledgements

I gratefully acknowledge the unconditional support of both my parents and my sister Martha towards the successful completion of this stage in my life, especially to my dad near the end, to whom I dedicate this work. Without them this would just simply not have been possible. My mother and Brittany Jack are dearly thanked for their invaluable emotional support thought my studies. I also express my gratitude to M.Sc. Gabriel Kerekes for his assistance during the laser scanned data collection. And last but not least, to my mentor Dr. Matilde Balaguer, whose help and guidance significantly improved the original manuscript with her corrections, suggestions and comments.

# Abstract

The present project is inspired on the rapid loss and damage of cultural heritage assets where the photogrammetric knowledge serves a clear goal documenting every detail of any structure, so as to preserve historic memorials. This project aims to reconstruct a detailed 3D model through the use of close range photogrammetry enhanced by laser scanning data acquisition. The monument that has been documented is found in the city center of Stuttgart, Germany, representing the Battle of Brienne.

A virtual 3D model of any cultural memorial, containing precise coordinates in a local system serves not only as a visually compelling model but also as an approach to obtain accurate measurements and analysis. It also preserves national heritage in case of destruction and can even be accessed or evaluated long distance. The techniques used can be extrapolated to record and/or to restore other monuments.

Various approaches will be explored in order to obtain the best and most accurate model possible. Starting from the use of different tactics in data capturing, continuing with the data processing, firstly, only by the means of Photogrammetry using, two different software, and later merging the obtained model with the laser scanned data recorded. The merged model is in advance expected to be more accurate, precise and complete.

This essay is structured firstly introducing the acquisition of the high-resolution data of the frieze along with the methods and equipment used, followed by some insights on the camera calibration performed. Afterwards, the result comparison from the different models obtained will be presented, this includes the usage of different software, the obtained model only by the means of Photogrammetry and also the merge model reconstructed with Laser scanned data. The drawbacks and strengths for each approach will also be explained. Finally, the metric features achieved will be presented and along with some conclusions and recommendations for future works in the same field.

# Resumen

El presente proyecto está inspirado en la pérdida acelerada y el deterioro de los bienes del patrimonio cultural, donde el conocimiento fotogramétrico sirve un objetivo claro documentando cada detalle de cualquier estructura a fin de preservar los monumentos históricos. Este proyecto tiene como objetivo reconstruir un modelo detallado 3D mediante el uso de fotogrametría de corto alcance, que será mejorado combinándolo con datos de escaneo láser. El monumento que se ha documentado, se encuentra en el centro de la ciudad de Stuttgart, Alemania, éste representa la *Batalla de Brienne*.

Un modelo virtual 3D de cualquier monumento cultural con coordenadas precisas en un sistema local, sirve no solo como un modelo visualmente atractivo sino también como UNA estrategia para obtener mediciones y análisis concretos. Este modelo también sirve para preservar el patrimonio nacional en caso de destrucción que incluso se puede acceder o evaluar a larga distancia. Las técnicas utilizadas para su generación pueden ser extrapoladas para documentar y/o restaurar otros monumentos.

Se explorarán varios enfoques para obtener el mejor modelo y el más preciso posible. Se comenzará empleando diferentes tácticas en la captura de datos, para seguir con el procesamiento de datos, en primer lugar, solo mediante el uso de fotogrametría de objeto cercano con dos programas informáticos diferentes y luego fusionando el modelo obtenido con los datos escaneados con láser. Se espera de antemano que el modelo fusionado sea más preciso, exacto y completo.

Este informe está estructurado en primer lugar, la adquisición de los datos de alta resolución del friso junto con los métodos y el equipo utilizado, seguido de algunas ideas sobre la calibración de la cámara realizada. Posteriormente, se presentará la comparación de resultados de los diferentes modelos obtenidos, esto incluye el uso de diferentes programas, el modelo obtenido solo por medio de fotogrametría y también el modelo de fusión reconstruido con datos escaneados con láser. Los inconvenientes y fortalezas para cada enfoque también serán explicados. Finalmente, se presentarán las características métricas logradas y junto con algunas conclusiones y recomendaciones para trabajos futuros en el mismo campo.

# Table of Contents

# Table of Figures

# List of Tables

# PART I

## 1. Introduction

A large variety of applications from the field of geomatics have been adopted in industries as diverse as medical, gaming, cinema, tourism, cultural heritage as well as in specific areas such as urban modeling, environmental planning and monitoring (Balsa-Barreiro and Fritsch 2018), road infrastructure mapping, industrial automation (Yang, et al. 2018), among others. The critical need for rapid and reliable information extraction and modeling of complex environments (Yang, et al. 2018) combined with the constant improvement in computational capacity and the use of new procedures for both collection and processing of geospatial data, has fostered during the last years the usage of three dimensional virtual models (Balsa-Barreiro and Fritsch 2018) (henceforth 3D models).

Taking into account that one of the main objectives of geospatial data collection and processing is the generation of realistic products of high resolution that include accurate descriptive and metric information, the most accepted optimal solution to generate those 3D models for different environments is nowadays the combined use of Terrestrial Laser Scanning and photogrammetric techniques (Balsa-Barreiro and Fritsch 2018). Consequently, in recent years, photogrammetry, remote sensing and spatial information have shifted from separate processing of obtaining information from imagery and point clouds to combined processing (Heipke, et al. 2016) and so 3D surface models from point cloud processing continue to gain increasing importance (Yang, et al. 2018).

The virtual modeling of complex and detailed cultural heritage assets, which have a high value due to their patrimonial heritage, is one of the current goals for recording and documentation. These scalable 3D models of historical objects can be used for future integration into complete virtual environments. In many cases, viewers are still limited to models based on only one geometric primitive while the combination of point-base models and mesh models with high-resolution textures in one is still not available, making the adequate presentation of documented cultural heritage an ongoing challenge (Mayer, et al. 2011). This is possibly due the requirement of high manual workload for data being collected at ground level and also for the digital reconstruction and data processing (Balsa-Barreiro and Fritsch 2018).

Given that this photogrammetric techniques can be extrapolated for the generation of large scale 3D urban models for instance, and the fact that real-world cases can be found in the different visual qualities in the 3D building models offered by institutions like Google (Balsa-Barreiro and Fritsch 2018), it is imperative to acquire some experience in this area of geomatics as a part of a possible employment option. In order to stay in line with the current cultural heritage preservation needs, the real-world object selected for 3D reconstruction in this present exercise, is of equal complexity and high detail as many historical facades, found in cathedrals, churches and alike.

## 1.1. Main Objectives

This project aims to generate a realistic 3D model of the northern frieze of a monument located in the city center of Stuttgart - Germany, which represents *the Battle of Brienne*. This frieze has been documented making use of two modern technologies: Close-Range Photogrammetry (henceforth CRP) and Terrestrial Laser Scanning (henceforth TLS). Within this framework, it is intended to specifically achieve the following:

- ✓ To reconstruct a photorealistic 3D model of the frieze with high resolution from the data acquired through CRP and TLS.
- ✓ To acquire spatial data from a real-world medium-size object by the means of digital CRP and TLS.
- ✓ To process the datasets acquired so as to generate realistic 3D models for later comparison and analysis.
- ✓ To implement an empirical new approach in the data acquisition phase, in order to explore the limits of the existing methodologies and to analyze the obtained results by the means of dense point cloud comparison.
- ✓ To draw relevant conclusions and applicable recommendations for projects of similar nature.

# PART II

## 2. Theoretical Framework

Successful 3D reconstruction from 2D imagery and laser-scanned point-clouds is achieved through various steps involving mostly principles from Close Range Photogrammetry (for the present scenario) and some concepts from the Computer Vision domain. Given that all the theories and models involved are of common knowledge and a detailed explanation can be found in multiple textbooks, only the main concepts will be explained in general terms. The matter of georeferencing terrestrial laser scanning is outside the scope of the present project.

### 2.1. Basic Concepts

#### Photogrammetry, Analytical Photogrammetry and Close Range Photogrammetry:

*Photogrammetry* is the art, science and technology of obtaining reliable information of physical objects through the process of recording, measuring and interpreting photographic images (American Society of Photogrammetry 1980). *Close Range Photogrammetry* (henceforth CRP) is applied only when the distance from the camera to the object of interest ranges from several meters to about 300 meters (Williamson, 2009). *Analytical photogrammetry* is the term used to describe the rigorous mathematical calculation of point coordinates in object space based upon camera parameters and measured coordinates of photos and on ground control, it also accounts for any tilts that exist in the photos and in general it involves the solution of large, complex systems of redundant equations by the method of least squares, which is possible thanks to the evolution of computer technology. The algorithms derived from this mathematical adjustment form the basis of many modern hardware and software systems (Wolf, et al. 2014). In conclusion, it is through photogrammetry that a quantitative analysis of image measurements is achieved, so as to reconstruct 3D objects with metrical properties (Cramer, 2017). The terms photograph and photo are used in this dissertation as synonymous of digital image.

## The photogrammetric process

In general terms, the digital image is measured and interpreted with methods that allow the identification of individual object points that have distinctive radiometric values (intensity, grey or colour value) and geometric data (position in the image). These measurements are then used in a mathematical transformation, between image and object space that is required for the object to be modeled. In order to achieve the 3D reconstruction, the measurement systems must have the appropriate geometric and optical quality. Figure 1 illustrates the reconstruction process from 2D digital imagery to the 3D virtual model, where human knowledge, experience and skill play a significant role in determining the extent to which the reconstructed model corresponds to the captured with digital images (Luhmann, et al. 2006).

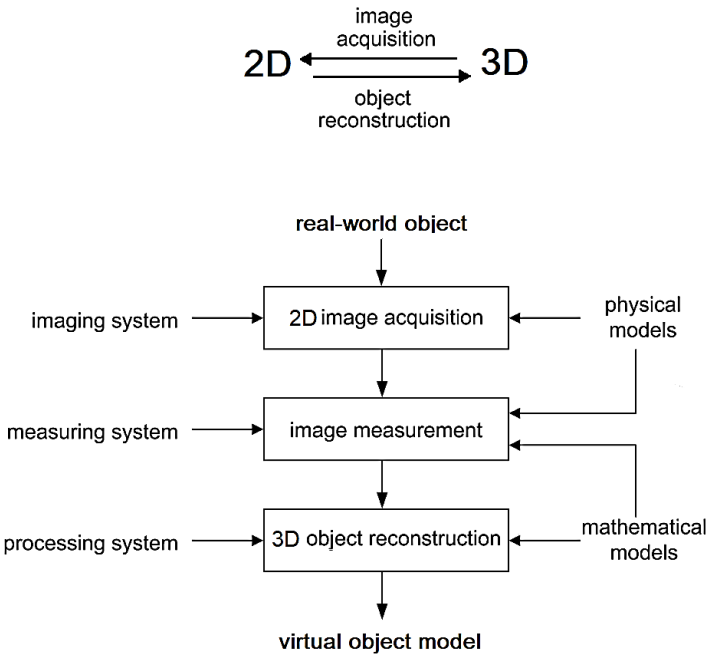


Figure 1. The Photogrammetric Process (Based on source Cramer, 2017 and Luhmann, et al. 2006)

## Stereoscopic Viewing

It is the perception of depth through binocular vision; it enables the formation of a three-dimensional stereo-model by viewing a pair of overlapping photographs or scenes. Stereoscopic depth perception is of fundamental importance in highly precise photogrammetric procedures, given that based on depth perception by comparisons of parallactic angles (formed by the intersection of the optical convergent axes) heights determinations and terrain variations can be studied in 3D. The nearer the object is to the viewer or camera, the greater the parallactic angle and vice versa (Wolf, et al. 2014). Stereoscopic viewing is an essential condition to make 3D modeling possible.

## Parallax

Is the apparent displacement in the position of an object, with respect to a reference frame, caused by a shift in the position of observation. Excessive amounts of parallax prevent stereoscopic viewing altogether (Wolf, et al. 2014).

### Lens Distortion

Occurs when light rays passing through the lens are bent, thereby intersecting the image plane at positions deviant from the norm. This deteriorates the positional accuracy of image points located on the image plane. Two types of lens distortion exist. The *Radial or symmetric lens distortion* causes imaged points to be distorted along radial lines from the principal point *o* (point of symmetry shown in the figure 2. Its effects throughout an image can be approximated using a polynomial. *Tangential lens distortion* occurs at right angles to the radial lines and is much smaller in magnitude. The effects of both are commonly determined during the camera calibration procedure (Gisresources n.d.). In Figure 2 both types of distortion are represented; Δr symbolizes the radial distortion along a radial distance r from the principal point *o*. The 3 coefficients k0, k1, and k2 are computed using statistical techniques, so as to be able to correct each measurement taken on an image for radial lens distortion (Gisresources n.d.).

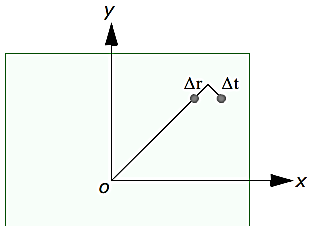


$$\Delta r = k_0 r + k_1 r^3 + k_2 r^5$$

**Figure 2. Radial vs. Tangential Lens Distortion. Based on source (Gisresources n.d.)**

## 2.2. Mathematical Models

### Central Projection

It is a mathematical system to represent 3D objects and space on a 2D surface by means of straight lines that go through only one point outside that plane, the perspective center (Cramer, 2017). This fundamental projection is the foundation for the 3D reconstruction used nowadays. Both, shape and position of an object are determined by reconstructing bundles of rays from individual camera positions to their corresponding object points. The spatial direction of each ray is defined in the 3D object space by scaling the vector formed by each image point *p*, and its corresponding perspective center *O*, provided that the parameters needed are known: the camera imaging geometry[1] and the position and orientation[2] of the imaging system with respect to the object coordinate frame, as illustrated in Figure 3 (Gisresources n.d.). During reconstruction at least 2 scaled vectors (rays) from homologous points are needed to position their corresponding object point onto the object space. The central perspective assumes the ideal camera model (pinhole) with no ray distortion, it also adopts the straight line concept in both object and image space, however in reality, perspective distortion is shown when lines are not parallel in image space.

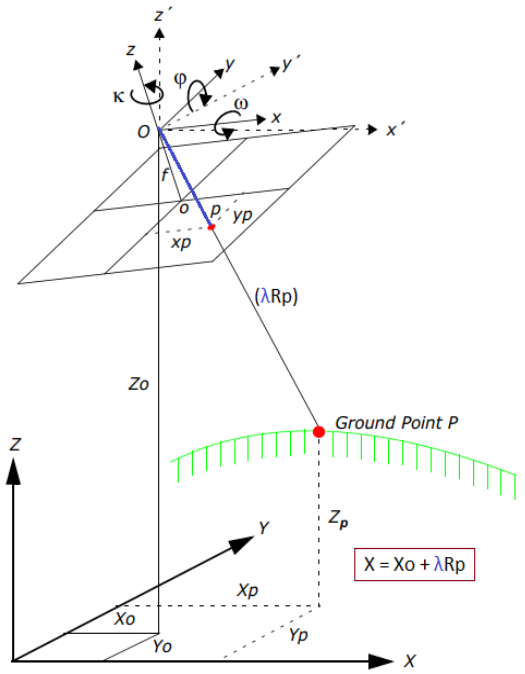


**Figure 3. Elements of Exterior Orientation. Based on (Gisresources n.d.)**



[1] Interior Orientation: is the internal geometry of the camera, which is defined by the principal point *o*, the focal length *f* and the lens distortion parameters Δr and Δt (Cramer, 2017 and Gisresources n.d.).

[2] Exterior orientation parameters: defines the position and orientation of the camera in the object space.

### Collinearity model

This model relates the object to image coordinates based on the central perspective model. The known collinearity equations, for every point in every photo, form the basis for the ray bundle adjustment (Cramer, 2017).

### Bundle Adjustment

It involves two different procedures. On the one hand “spatial resection” for multiple images, which is the simultaneous estimation of all exterior orientations and all unknown object point coordinate; and on the other hand “forward intersection” that generates the corresponding rays to the same object point from stereopairs or multiple images that intersect at each individual point, thus calculating its object point coordinates.

## 2.3. Photogrammetric Modeling Methods

### Structure from Motion - SfM

As the name suggests, it is a method that recreates the structure of the study object based on the different positions and orientations (“the movement”) of the camera where the images were originally recorded. This low-cost photogrammetric method is nowadays used for high resolution topographic reconstruction. It automatically and simultaneously solves the cameras positions and the geometry of the scene. This is done by using a highly redundant bundle adjustment that is based on matching features in multiple overlapping offset images (Westoby, et al. 2012). In other words, the Structure-from-Motion method operates under the same basic concepts of stereoscopic photogrammetry, but it differs in the fact that the geometry of the scene, camera positions and orientation are solved automatically and specially without an initial network of targets with known 3D positions. Instead, SfM solves them simultaneously making use of a highly redundant and iterative bundle adjustment, based on multiple features automatically extracted from a set of overlapping images (Westoby, et al. 2012).

A number of cloud-processing engines have dramatically popularized this approach together with the development of automatic feature-matching algorithms. The principles of this powerful methodology include the determination of the 3D location of points within a scene. This means that the 3D location and pose of the camera are required, and thus a solution through triangulation can be used to reconstruct the geometry of the original scene. Automatic identification of matching features in multiple images is tracked from image to image, providing with initial estimates of camera positions and object coordinates. This is then refined iteratively using non-linear least-squares minimization (Westoby, et al. 2012).

A typical object reconstruction process using the SfM method starts by (1) locating key points or homologues features between different images a Scale-Invariant Feature Transform (SIFT) operator can also be used for this task. The process continues with (2) the sparse point cloud computation, calculating the internal and external orientation, and (3) the dense point cloud generation which thickens the point cloud. The last step is (4) the post-processing and final elaborations (Caradonna, et al. n.d.).

Normally a transformation is used to change image-space coordinates to an absolute coordinate system. A 3D similarity transform based on a small number of known ground control points (GCP) can be used with known object-space coordinates to achieve this goal. These GCP can be identified afterwards with candidate features that need to be clearly visible in both the resulting point cloud and in the field. To make this task easier it has been standardized the use of physical targets with a high contrast and clearly defined centroid in the field before acquiring images. This approach simplifies the unambiguous co-location of image and object space targets. As it is known, is useful and recommended to incorporate a degree of redundancy in the GCP network.

Photogrammetric point clouds can be generated by using stereo image matching and multi-view stereo techniques, which can be applied to close range imagery (Balsa Barreiro, 2018). These in turn enable to generate 3D point clouds by using photogrammetric techniques.

It can also be noted that SfM can determine the orientations and positions from where each image was captured, whereas the SIFT operator can identify potential features for matching (Balsa Barreiro, 2018). The final verification for each match is achieved by finding the low residual least-squares solution for the unknown parameters of the model (Westoby, et al. 2012). Afterwards, a procedure for bundle block adjustment of the images is carried out so as to compute a sparse 3D point cloud in the photogrammetric software. Finally a RANSAC robustness estimator is applied for the detection of outliers and for filtering mismatches with the point clouds in question (Balsa Barreiro, 2018).

# PART III

## 3. Project Design and Documentation Requirements

It is planned to reconstruct a 3D model of high accuracy and resolution of a medium-size cultural heritage asset from spatial data acquired through CRP and TLS. The intended accuracy is of a subpixel level for all measurements. The most relevant aspects related to each procedure involved, are described in the following sub-sections. This includes the equipment and computational requirement followed by the documentation and processing of data.

### 3.1. Study Object

The object selected for the photo-realistic 3D reconstruction is characterized by a high concentration of relief figures of 14cm of depth on a frame measuring 5.50m wide and 1.05m high (figure 4). It is located on the northern frieze of the commemorating anniversary column located in the city center of Stuttgart in Germany. The monument has a high patrimonial value since it depicts *the Battle of Brienne held on February 1$^{st}$ 1814*. The access to the frieze itself needs to be taken into account not only because the column is surrounded by populated commercial markets, with crowds of people constantly present in the area, but also because the highest features are on the upper frame located 3.50m above ground. The frieze rests on a concrete base with 2 stairs and a distance of 1.20m from the highest step to the lower part of the frame. Moreover, several features are in the background which accounts for important areas of occlusion for the appropriate documentation of details.

Figure 4. Perspective of the Study Object

## 3.2. Documentation Strategy

Given that a high level of photorealism and visual completeness in the final 3D model are required, for some datasets the known recommendations for an optimal data acquisition with CRP will be taken into account (Wenzel, et al. 2013). On the other hand, so as to consider some real life situations and to explore the limits of the existing methodologies and modern photogrammetric techniques, other datasets will use a different scheme rather than the usual photogrammetric recommendations in order to adopt a crowd-source imagery input approach. The latter will be explained in the forthcoming sections.

### Favourable conditions for data acquisition:

- The lighting conditions should be such that the material is diffusely illuminated; possible reflections should be always avoided and sufficient light should be available for all parts of the scene, especially those in the background.
- The photographer should ensure the complete coverage of the frieze during the data acquisition phase; i.e. all points of interest must be clearly visible on the resulting images.
- Given that the object has a complex surface, small baselines are needed specially to ensure that potentially occluded parts are visible in at least 3 images.
- The object should be captured from different viewing angles.
- Pre-calibration of the camera: even though there is no absolute certainty that the camera parameters will not change between the lens calibration and the capture of images, since this is done at different physical locations. Calibrating the camera is a useful precaution in case the software fails to calculate the distortion parameters for any reason or there is a problem with the tie-points it bases on for this purpose.
- In order to avoid problems due to the different focal lengths in the photographs, the automatic adjustments should be disabled, using preferably a fixed focal length and no image stabilization.
- The type of lens to use should be preferably a wide angle, which is better than narrow angle, due to the small focal length requirement.
- After or during the acquisition it is advisable to examine all the photos in order to avoid color distortions and blurriness.

Many of the recommendations given above, are adapted from (Wenzel, et al. 2013) for the first part of this specific exercise.

## 3.3. Equipment Used

### 3.3.1. Comparison TLS vs. CRP

Given that the most accepted optimal solution to generate realistic 3D models for different environments is nowadays the combined use of Terrestrial Laser Scanning and photogrammetric techniques, in this academic exercise both will be explored. The use of photogrammetric techniques and laser scanning techniques differ corresponding to their performance in different tasks. Photogrammetric techniques are preferred for acquiring color and texture information, for generating not only precise 3D data from multiple 2D images captured in different positions and orientations, but also point clouds by using stereo image matching and multi-view stereo techniques. Compared to other survey methods, the low cost and performance of digital cameras, aid in scientific research, given that these can capture geometric and radiometric information from the images with high resolution and accuracy by means of optimal image repetition rate (Balsa-Barreiro and Fritsch 2018, 2).

Laser scanning systems, on the other hand, generate large volumes of data at incredibly fast rates with high redundancy, although these systems may present some drawbacks related to their operational costs and their technical performance under certain circumstances such as restricted narrow areas. Furthermore, the data collection of some linear elements and materials, such as glass buildings, are often left incomplete and, similarly, some of these systems cannot obtain color images or they do worse than photogrammetry (Balsa-Barreiro and Fritsch 2018, 2).

A photogrammetric workflow comparison is shown below in figure 5 versus the one typically followed with TLS, which is shown in figure 6.

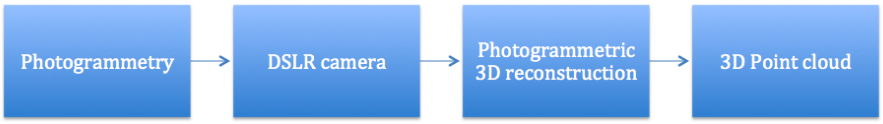


Figure 5. Photogrammetric Workflow (Rodríguez-Gonzálvez, et al. 2017)


Figure 6. TLS Workflow (Rodríguez-Gonzálvez, et al. 2017)

Figure 7 shows the different categorization for both non-contact measuring methods.

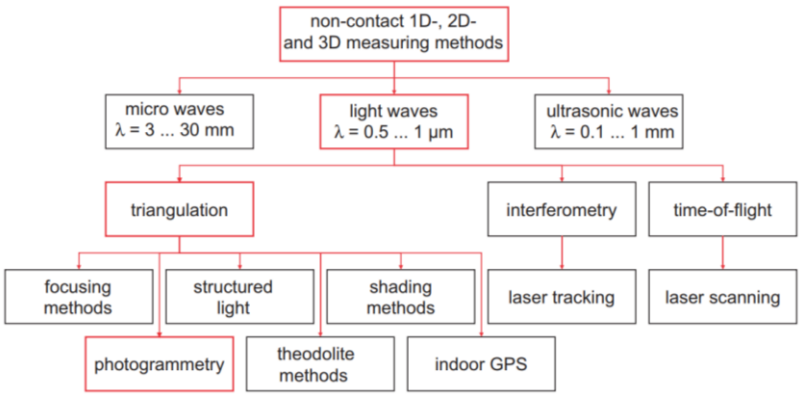


Figure 7. Categorization of Non-Contact Measuring Methods (Luhmann, et al. 2006)

### 3.3.2. Cameras

A digital single-lens reflex camera (DSLR) uses a mirror and prism system that allows the photographer to see exactly what will be captured through the viewfinder of the camera. With other type of lenses the image viewed is somewhat significantly different than the one captured as the final image (Benefits DSLR Portraits , 2019).

Digital cameras have been used for photogrammetric measurement for over 25 years (Luhmann, et al. 2016) and from experience it is known that a key factor in determining the final texture on the model is the high resolution. This is ensured by making use of a DSLR camera that delivers better sharpness, clarity and of course resolution.

So as to mimic the crowd-source approach two different cameras were used. Some general features of both cameras used are given in the table below (table 1).


Figure 8. Camera Sony A7 II (Sony, 2019)


Figure 9. Camera Nikon P500 (Nikon, 2019)

| | Sony A7 II | Nikon Coolpix P500 |
|---|---|---|
| Sensor | Full frame CMOS | 1/2.3" CMOS |
| MP | 24MP | 12MP |
| ISO | 100 - 25600 | 160 – 3200 |
| Sensor-shift Image Stabilization | Yes | Yes |
| Tilting Screen | 3” | 3” |
| fps continuous shooting | 5.0 | 1.0 |
| Electronic viewfinder | 2359k dot | Yes |
| Zoom Lens | | 23–810 mm F3.4 - F5.7 |
| Body | 599g. 127 x 96 x 60 mm | 494g. 116 x 103 x 84 mm |
| Other Features | Weather Sealed Body | |
| Video Resolution | 1920 x 1080 | |

Table 1. Camera Features

### 3.3.3. Laser Scanner

HDS7000 Ultra High-Speed, Phase Scanner


Figure 10. Leica HDS7000 Laser Scanner (Hartman, 2019)

| Properties | Leica HDS7000 3D Laser Scanner |
|---|---|
| Type of scanner | Compact, phase-based laser scanner |
| Camera | No integrated camera |
| Dim. / Weight | 286 mm D x 170 mm W x 395 mm H / 9.8 kg, nominal |
| Type | Phase-shift |
| Wavelength | 1.5 µm (Invisible) |
| Range | 187 m ambiguity interval; 0.3 m minimum range; 0.1 mm resolution |
| Linearity error | ≤ 1 mm |
| Beam divergence | < 0.3 mrad |
| Scan rate | Up to 1,016,727 points / sec, maximum instantaneous rate |
| Scan resolution | QUALITY / LOW / NORMAL / HIGH / PREMIUM / PTS/360º (VERT/HORIZ)<br>Preview / 0:13 min / 0:26 min / 0:52 min / 1:44 min / 1250<br>high / 1:44 min / 3:22 min / 6:44 min / 13:28 min / 10000 |
| Field-of-View | max. 360Æ x 320Æ (horizontal / vertical) |
| Scanning Optics | vertical rotation speed (6.25 rps, 12.5 rps, 25 rps or 50 rps); Environmentally protected by shield |
| Angular accuracy | 125 µrad / 125 µrad (horizontal / vertical) |
| Angular resolution | 7 µrad / 7 µrad (horizontal / vertical) |
| Level indicator | Electronic bubble in onboard control and software |
| Data storage | 64 GB flash drive (integrated), 2 x 32 GB USB flash drive (external) |
| Communications | Ethernet or integrated Wireless LAN (WLAN) |
| Data check | Self-check at startup (Data Integry Monitoring) |
| Battery Type | Internal: Li-Ion |
| Duration | Internal: > 2.5 h , AC power supply: unlimited |
| Hardware Options | HDS scan targets and target accessories |

Table 2. Leica Laser Scanner Features

Phase-based scanners (figure 10) are known for their ultra-high scan speeds and corresponding high scan density, but have long been relegated to short range, as-built applications such as tunnels, building interiors, and compact industrial plants. It has scanning speeds up to >1 million pts/second. The HDS7000 phase-based scanner extends the practical range at which phase-based lasers can receive detectable laser returns – especially from vertical surfaces. In the past, such practical maximum return limits were around 60m – 70m. For the HDS7000, this range is more than 100m. Depending on site logistics, extended range can reduce the number of scanner setups needed on certain projects.

### 3.3.4. Accessories

The following accessories were used:

- A tripod, to aid with stability avoiding blurriness in the photographs and also to ensure the same distance to the object and between camera positions.
- Non-reflective Targets (black and white tilt-and-turn targets) were deployed to co-register the TLS data.
- Target`s holders and tripods, for the targets self-stability.
- Extra batteries, for both the scanner and cameras.
- Casings, for safeguarding the used equipment.
- Construction tape, to mark the restricted area.

## 3.4. Software and Hardware Used

### 3.4.1. Software

- Leica Cyclone 8 was used for the laser scans data registration.
- Agisoft Lens was needed to automatically calibrate the cameras.
- Agisoft Photoscan was used for generating sparse and dense point clouds from imagery.
- RealityCapture was used for the combined data processing of imagery and registered point clouds from laser scanner.
- CloudCompare was used for the comparison of the end results obtained with the previous photogrammetric software.

### 3.4.2. Hardware

Given that a number of combinations of settings and photographs is anticipated to be rendered for different outputs, it is advisable to work on a computer that surpasses the minimal requirements given by the software manufactures. The RealityCapture software for instance, recommends to run on x64bit machines with at least 8GB of RAM and imperatively an nVidia graphics card with Cuda 2.0+ and a GPU of at least 1GB RAM, since RealityCapture uses the GPU for calculating depth maps and alike. This aspect will be discussed further in the results section.

# PART IV

## 4. Methodology

The following paragraphs, will explain the methodology in detail followed in the present work. Figure 11 displays a summary of the implemented workflow.

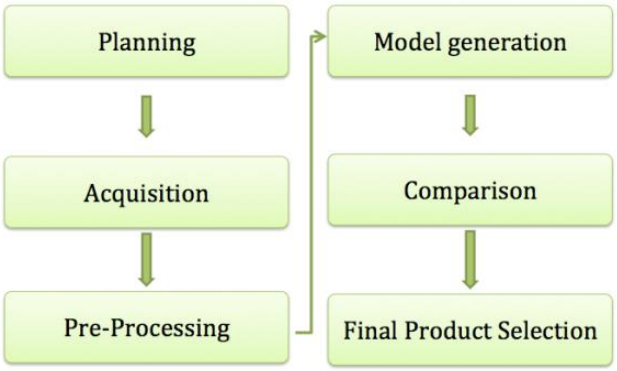


Figure 11. Methodology Workflow Overview

Figure 12 shows the detailed yet summarized implemented workflow, the step by step process from the project planning phase up to the pre-processing or data preparation. The complete workflow diagram can be found in the appendix section. The self-explanatory steps that are mentioned in the workflow will not be further discussed. Firstly, the data collection and preparation will be exposed, followed by the processing of CRP data and subsequently the merged process with the LS point cloud.

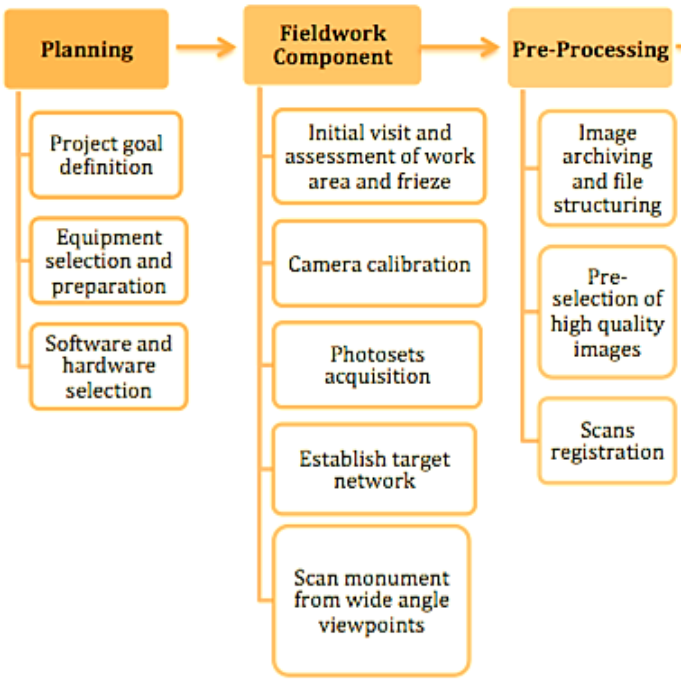


Figure 12. Methodology Detailed Workflow

## 4.1. Data Collection

### 4.1.1. Photogrammetric Data Collection

Two main datasets were captured. One takes into account the known recommendations for an optimal data acquisition with CRP previously discussed and the other, adopts what in this document will be called a "crowd-source" imagery input approach. The first photoset represents controlled situations where preliminary planning is performed and where factors such as: camera orientation, distance between baselines, lighting or full object coverage can be monitored. The three main considerations for pictorial quality: resolution, depth of field, and exposure (Wolf, et al. 2014) can also be taken into account. The second photoset represents use a different scheme rather than the usual photogrammetric recommendations.

This combined input approach was adopted for two main reasons. Firstly, in real case scenarios many close-range photogrammetric analyses are done with existing amateur photography. For example: vehicle accident scenes, forensic or archaeological surveys where a photogrammetric analysis may be needed to determine evidence or facts. Such photography may not be ideally exposed, well focused or, generally speaking, in an optimal geometric configuration for photogrammetric analysis (Wolf, et al. 2014). The second reason is because now that many of the previous hurdles in automated 3D modeling have been solved, the apparently trivial question of image matching, equally as effortlessly as human observers can, is still unsolved and represents one of the major limitations to automatically find correspondences for large-baseline views (Hartmann, et al. 2016) and especially for big changes in perspective, where the SfM methodology has some room for improvement. To recap, the second photoset representing a crowd-source approach input is taken as an exercise to evaluate the evolution of well-guarded newly implemented solutions in commercial photogrammetric software, in regard to the still unsolved issue of image matching as human observers previously mentioned.

The photographs captured have been categorized in 3 Batches as explained in table 2 below. This was done so as to categorize the photogrammetric vs. the crowd-source approaches.

| | PhotoSet 1 (PS1) | PhotoSet 2 (PS2) | PhotoSet 3 (PS3) |
|---|---|---|---|
| Dataset/ Approach | Crowd-Source Input | Photogrammetric Planned | Crowd-Source Input |
| Camera Used | Sony A7 II & Nikon Coolpix P500 | Nikon Coolpix P500 | Nikon Coolpix P500 |
| No. Photos Captured | 127(Sony), 78(Nikon) | 401 | 102 |
| Acquisition Situation | Pre-Acquisition Test | Extended photo capture | Capturing of TLS Data and Targets |
| Acquisition Time | 53m | 2h 15m | 15m |
| Distances to Object | Different | Constant | Different |
| Baseline Distance | Constant, approx. 1m | Constant, approx. 1m | Multiple, >1m |
| Viewing Angles, Perspectives | Multiple | Multiple. Systematic | Multiple |
| Estimated Image Overlap | Sony 50%, Nikon 70% | 80% approx. | 60% approx. |
| Coverage Of The Frieze | Partial 80% | Total | Total |
| Camera Pre-Calibration | Performed for Nikon | Performed | Not Performed |
| Automatic Adjustments | Close-up Scene, ISO400 (Sony) | Disabled | Close-up Scene |
| Image Stabilization | Disabled | Disabled | Disabled |
| Fixed Focal Length | Disabled | Enabled | Disabled |
| Accessories Used | None | Tripod | Targets |
| Climate | Winter, Cloudy (-5°), Sunny (Nikon) | Winter, Snowy (2°) | Summer, Sunny(30°) |
| Lighting Conditions | Natural Light Photoflash Disabled | Natural Light Photoflash Disabled | Natural Light Photoflash Disabled |
| Photo Examination | Not Executed | Executed | Executed |
| Software For Processing | Agisoft PhotoScan | PhotoScan and RealityCapture | PhotoScan and RealityCapture |

Table 3. CRP Photosets Organization and Categorization

It needs to be mentioned that in only 2 measurements were taken from the frame of the frieze to get an approximate scale, given that the exact measurements were goint to be extracted from the subsequent TLS data acquisition.

### 4.1.2. Data Collection with Laser Scanner

Taking into account the description of the study object given in the corresponding section, the acquisition with laser scanner was planned so as to assure the occluded areas were captured as much as possible, and also to block the continuous influx of visitors in all directions. Figure 13 offers a general view of the restricted area can be seen and figure 14 shows the different scan positions adopted with wide angle perspectives and distances from the monument.

For the successful acquisition of data, all the equipment needed was prepared and packed beforehand: primarily the scanner, making sure it was charged and functioning; the 7 non-reflective targets that were deployed to co-register the TLS and CRP data, and all accessories such as the tape to mark the restricted area, the casings, the target´s holders and tripods required for their self-stability.

During the field campaign, the scanner firstly performed a pre-scan in low definition to determine positioning in less time and then the option of window selection was selected so as to have faster scans and processing and less data density in the surrounding areas of the monument. It must be noted that although previously checked, during this acquisition the scanner malfunctioned showing a battery related error after each pre-scan and had to be rebooted to complete the whole process successfully. Also, the scanner´s screen visibility was greatly restricted due to the direct sun´s reflection. For future deployments a tablet for remote scanner command is highly advisable.

Figure 13. General View of the Restricted Area and Target Placement

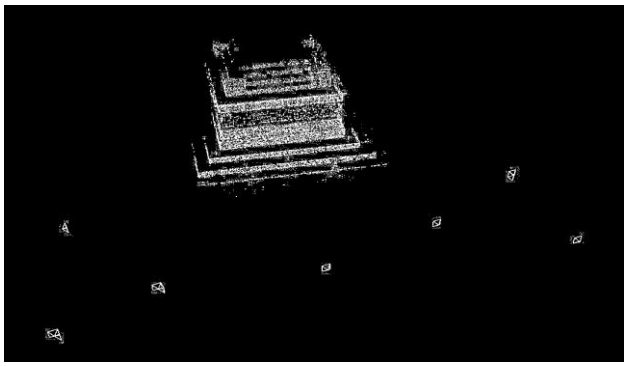

Figure 14. Scan Positions

## 4.2. Data Preparation

After the data acquisition, the scans were registered using the software Leica Geosystems Cyclone 8. The use of targets was compulsory to complete this task. The registration was closely inspected in CloudCompare and one of the viewpoints was removed due to an alignment issue that is shown in figure 15. This may have been caused during the manual selection of target center points. The remaining scanned positions were exported to a new file.

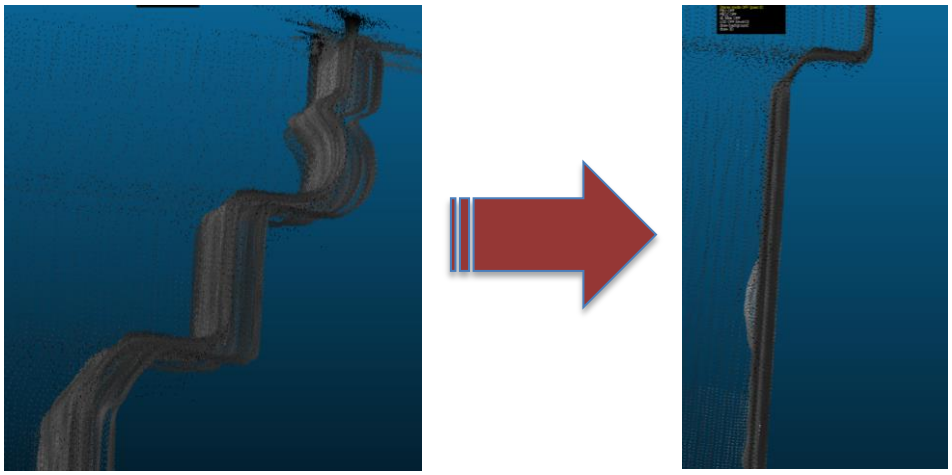

Figure 15. Alignment Correction

With regard to the imagery, some photos that presented blurriness, lack of sharpness or were greatly obscure were deleted from the final input file. Examples of which can be seen in figure 16.

Figure 16. Low Quality Photo Filtring

In addition, a specific organized structure of the folders was created in the workstation, so as to access the data easily and to remember under what criteria the files were created; for instance the numerous model trials that involve different settings.

### 4.2.1. Camera Calibration

Generally speaking, it defines the internal geometry of the camera or sensor, as it existed at the time of the image capture (Gisresources n.d.). In other terms, it delimits the variables within the interior orientation, which include: the calibrated focal length, the calibrated principal point coordinates (also known as the point of best symmetry), the coefficients of symmetric radial lens distortion and decentering distortion. Their most probable values are computed with a least squares mathematical model (Wolf, et al. 2014). The interior orientation must be determined by calibrating every camera and for each focal value if it is a zoom objective (Luhmann, et al. 2006). It is primarily used to transform the image pixel coordinate system to the image space coordinate system (Gisresources n.d.).

### 4.2.2. Automatic Calibration Software

Agisoft PhotoScan has its own software to automatically calibrate the cameras, the Agisoft Lens. It includes its own "*chessboard pattern*" with instructions to be captured from different angles with the same camera that would be used to record the imagery. This can be seen in figure 17. The chessboard pattern provided was captured 12 times from different orientations, only a sample is shown.

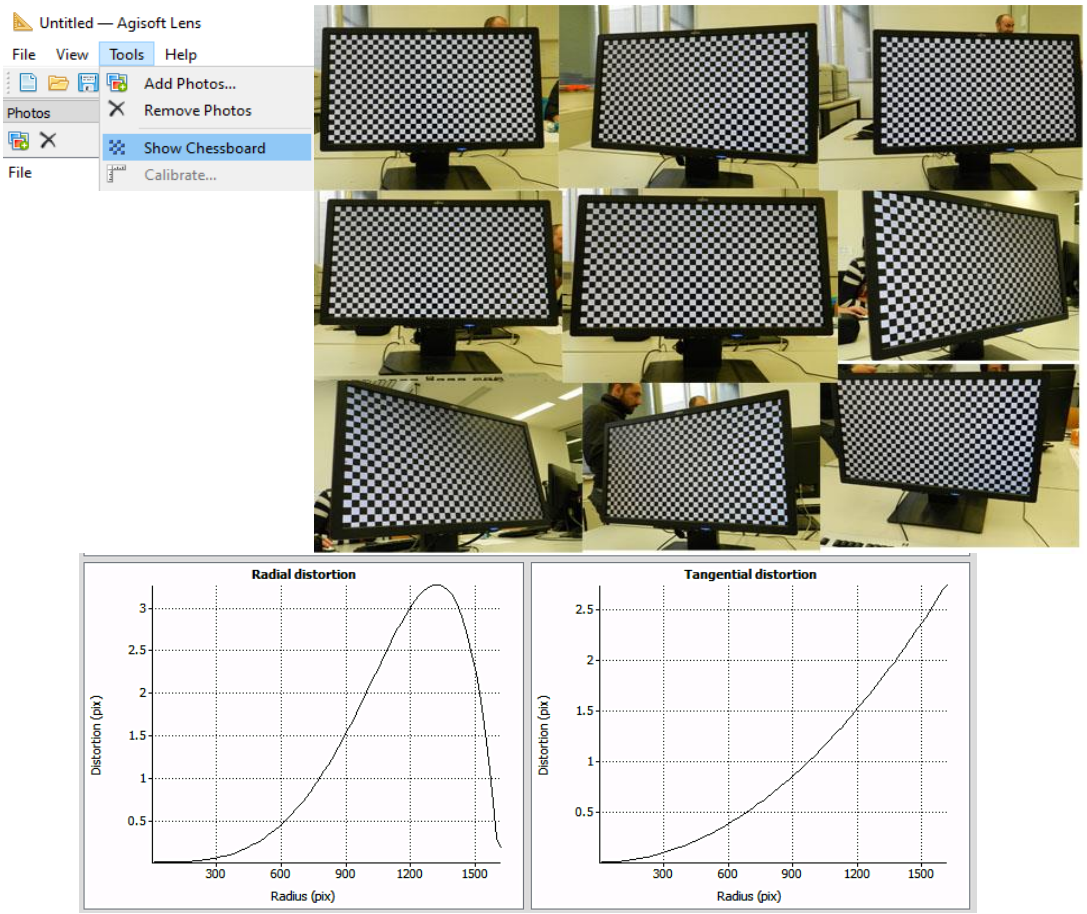


Figure 17. Agisoft Lens Calibration Pattern and Report

As a complementary learning exercise, the “Cameracalibrator’’ in Matlab was also launched with the same 12 images as input, although here only 8 were registered. This is displayed in figure 18 below.

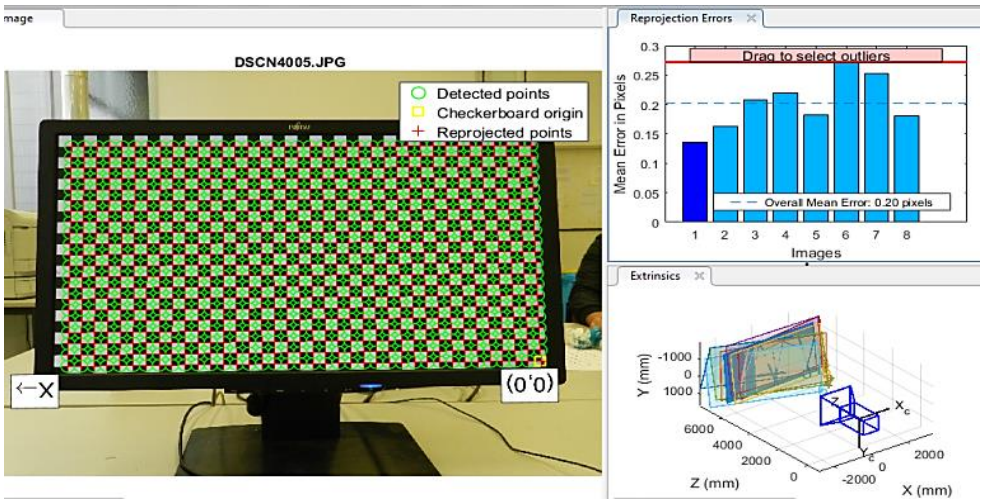


Figure 18. Matlab Calibration Pattern and Report

After the camera calibration process finishes, both computational solutions generate a report with the calibration parameters obtained; this is shown in figure 19. As it can be seen, the obtained calibration parameters in both are approximately the same, although that can only be assumed from the resulting values given that the specific method or algorithm used to calculate them is not known for either software. In Matlab, it is useful to see the detected and reprojected points and the over imposed input images are used to determine the estimated location of the principal point and specially the selected origin, because its coordinates vary in the y-component compared to the results given by Agisoft. They differ greatly specially in the radial component.

| Parameter | Value | Std Error |
|---|---|---|
| Image width | 3264 | |
| Image height | 2448 | |
| Focal length | 3167.5 | 0.976378 |
| Principal point (x) | -16.1884 | 1.10396 |
| Principal point (y) | -24.2038 | 0.751683 |
| Affinity B1 | -0.734366 | 0.16269 |
| Skew B2 | 0.777399 | 0.14532 |
| Radial K1 | 0.0189278 | 0.00510528 |
| Radial K2 | 0.068181 | 0.0732659 |
| Radial K3 | -0.547944 | 0.410525 |
| Radial K4 | 1.00468 | 0.604967 |
| Tangential P1 | -0.0014471 | 0.000126391 |
| Tangential P2 | -0.00298922 | 7.83154e-05 |

```
Camera Intrinsics
                IntrinsicMatrix: [3x3 double]
                    FocalLength: [3.1716e+03 3.1723e+03]
                 PrincipalPoint: [1.6091e+03 1.2018e+03]
                           Skew: 0.6278

Lens Distortion
             RadialDistortion: [0.0265 -0.0296 -0.0201]
          TangentialDistortion: [-0.0028 -0.0021]
Camera Extrinsics
             RotationMatrices: [3x3x8 double]
          TranslationVectors: [8x3 double]

Accuracy of Estimation
        MeanReprojectionError: 0.2017
           ReprojectionErrors: [798x2x8 double]
            ReprojectedPoints: [798x2x8 double]

Calibration Settings
                   NumPatterns: 8
                   WorldPoints: [798x2 double]
                    WorldUnits: 'mm'
                  EstimateSkew: 1
NumRadialDistortionCoefficients: 3
   EstimateTangentialDistortion: 1
```

Figure 19. Calibration Result Comparison (Agisoft and Matlab)

## 4.3. Data Processing

The photogrammetric software chosen, Agisoft PhotoScan and RealityCapture will be used to reconstruct the 3D model of the frieze. On the one hand, PhotoScan will be solely used for the image based surface reconstruction, whereas in RealityCapture both datasets, from CRP and TLS, will be added and registered to generate a final rendered model. A general workflow is shown in the diagram below in figure 20.

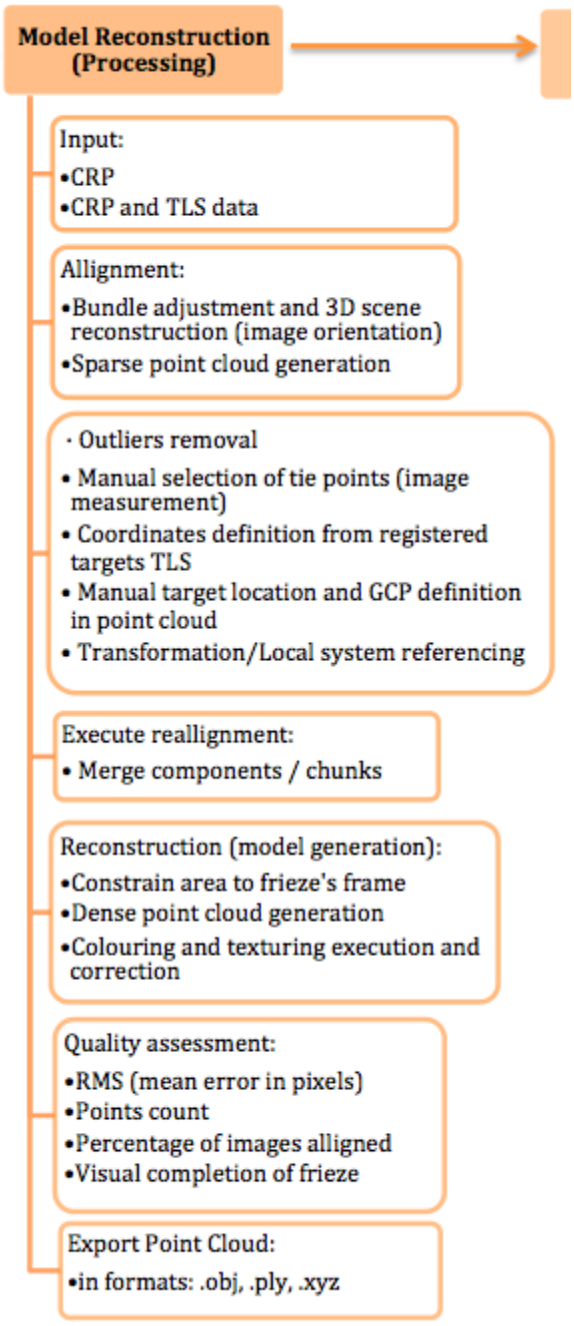


Figure 20. Data Processing Workflow

In general, any photogrammetric software has an equivalent workflow; first the data is imported and aligned; then, the individual components generated are merged using a manual selection of tie points and afterwards the reconstruction and generation of dense point cloud can be launched to conclude with texturization and coloring acquired from the inputted imagery.

Since it is operated with commercial software, it is not exactly known which specific algorithms are implemented in the processing. However, it is well known that during the alignment phase, a specific sequence is executed as follows:

1. To find prominent points in all images.
2. To find characteristic features of each point.
3. To link the corresponding tie points (relative orientation model) and use transformation of translations and rotations to orient the images with respect to each other.
4. To build the 3D projection rays and intersections with the corresponding homologous points, in order to locate the object point coordinates in the object space.

This procedure generates a sparse point cloud that describes the surface's shape continuously.

### 4.3.1. Photogrammetric Data Processing

The Agisoft PhotoScan software was exclusively used to process and reconstruct a model only based on photogrammetric input of all images in photosets 1 (PS1) and 2 (PS2). Some relevant models rendered will be discussed. The software workflow starts with the data input, followed by the alignment of cameras that generates the sparse point cloud and the reconstruction process from which the dense point cloud is derived. The process finishes when texture and color are applied to the rendered model.

It must be mentioned beforehand that in Agisoft Photoscan, the algorithm Dense Multi-View 3DReconstruction (DMVR), which seeks correspondence between each pixel of the photographs, enables the software to offer several levels of detail (lowest, low, medium, high, and ultra-high) at the beginning of each step of the reconstruction. The Ultra-high option processes with the original resolution of the photographs and at each of the following steps, the resolution is downscaled by a factor of 4 (pixel number divided by 2, in length and width)(Fau, et al. 2016).

Some of the processing settings and level of detail used within PhotoScan were:

- For batch PS1: Low quality and high/mild processing. Texturing: Generic & Mosaic.
- For batch PS2: High/mild quality processing. Texturing: Generic & Mosaic.

Various models were generated so as to analyze the photosets and to choose an optimal result of high accuracy and resolution. Firstly, the input images will be treated separately and afterwards the individually generated sparse point clouds will be merged.

The final selected model was segmented afterwards in Cloud Compare to remove non-desired additional noise. This will be shown in the comparison projects phase.

### 4.3.2. Processing Batch PS1 (All imagery from the Sony Alpha 7 Camera)

In the initial visit along with the preliminary assessment of the area, a sample of the frieze was captured in order to acquire initial information and to know the possible adjustments needed for the final model. The partially captured data mimics the crowd-source input for the Photo Set 1 (PS1). Covering the lower half of the frieze with approximately 50% overlap between photos, 126 photos were taken and processed in Agisoft Photoscan. Additionally, no measurements or pre-calibration of the camera was used at this point.

From this initial experimental processing some considerations were taken to improve the upcoming photogrammetric imagery campaign. For instance, regarding the weather, the automatic adjustment of the camera adapted a high ISO value to a noticeable brightness due to the cloudy obscure natural conditions. That resulted in a non-truthful color, thus not enabling this batch for later consideration in the coloring or texturing. Additionally the below zero temperatures caused the photographer to shake intensely, this constant vibration resulted in the blurriness and lack of sharpness for various photographs that had to be deleted. The “less cold” hour of the day had to be chosen as a precaution for the next image capture. A sample from the images is shown in figure 21 below.


Figure 21. Sample of Batch PS1

*Model Generation*: the initial crowd-source approach assumed the data captured only from frontal images with the strip method and a great overlap with approximately the same base between camera stations. As expected, given the detailed surface of the object and its 3-dimensionality, these images were not sufficient to capture all the occluded areas of the object, leading to great loses of information in the 3D model that were not recovered even with the hole filling option selected for building the texture. It must be noted that this experiment was intentional to check the software capabilities with different options and especially because at a later stage this batch is intended to be merged with other simulated photosets within the crowd-source approach.

Thanks to the great overlap all the 126 images were aligned; the reconstruction parameters were high quality mode and mild depth filtering. After a total of 59 minutes, the resulting model rendered with a reprojection error of 0.388 pixels. Samples of the model and reconstructed camera positions are shown below (figure 22).

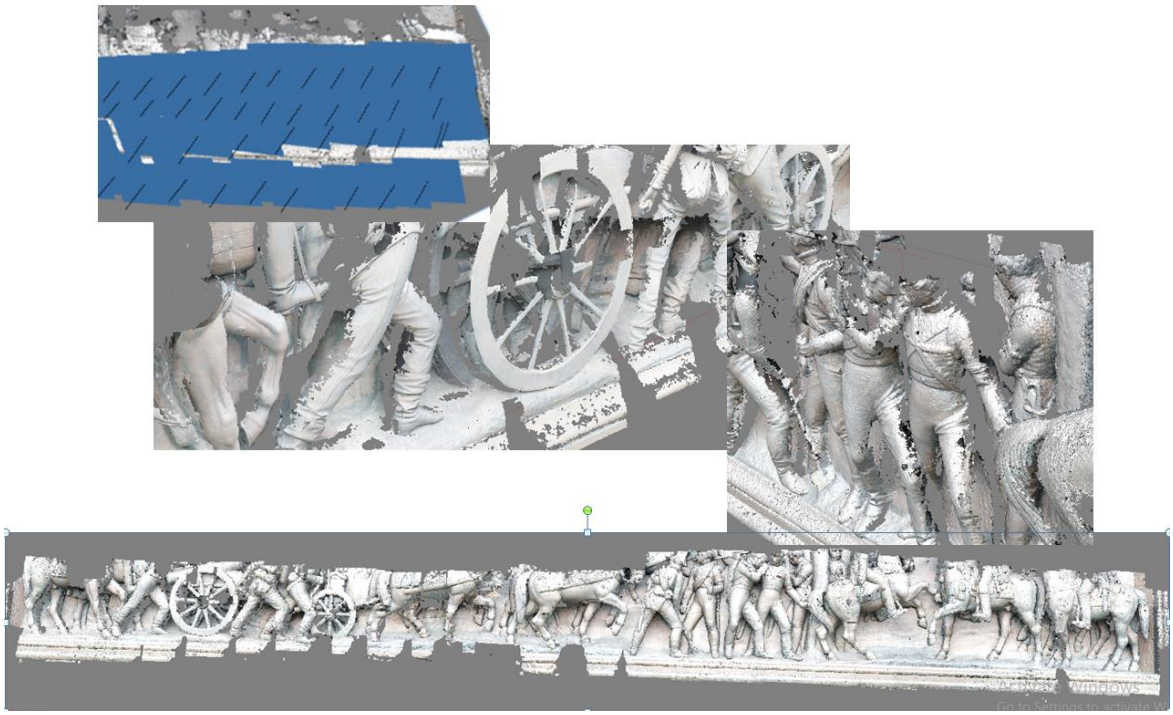

Figure 22. Batch PS1 Reconstruction and Camera Positions and Orientations

### 4.3.3. Processing of Batch PS1 and PS2 (All imagery from the Nikon Camera)

Taking into account the circumstantial blunders from the initial acquisition, some extra precautionary measurements were taken in addition to the recommended and planned photogrammetric tips for the optimal acquisition. The surface reflectance was also monitored.

Using the Nikon Coolpix P500 previously calibrated camera (exposed in the following section) and a 5.6 mm focal length, 401 images were captured throughout the frieze, with an 80% overlap and the aid of a tripod to guarantee stability. Following the suggested methodology by Wenzel et al in "One panorama each step" (2013), it was intended to capture every detail in the occluded areas with oblique images to the left and right and also to reduce the time of acquisition. These pictures were taken with 180° rotation of the camera mounted on the tripod per station and an approximate baseline of 1m between stations. This constitutes the **batch PS2** meant to follow most of the photogrammetric recommendations explained before.

Afterwards, the camera settings were changed to the close-scene mode and the focal length was not fixed so as to partially capture another part of the frieze and complement this way the photoset 1 (**PS1**) within the crowd-source input approach. A total of 78 images were taken with the strip method under these camera settings.

#### 4.3.3.1. Camera Calibration Residuals

The Nikon camera was used for photosets 1 (PS1) and 2 (PS2); they represent a crowd-source and a photogrammetric input correspondingly. The camera was calibrated before the acquisition. Figure 23 below, shows a comparison in image residuals from the camera calibration procedure. It can be seen that although different focal lengths were used, the images captured in both photosets have a subpixel reprojection error. It can be clearly be seen that the PS1 batch has the biggest residuals, possibly because it only registered 24 out of the 78 images taken for this photo batch, whereas in the PS2 batch 389 images out of 401 were aligned.

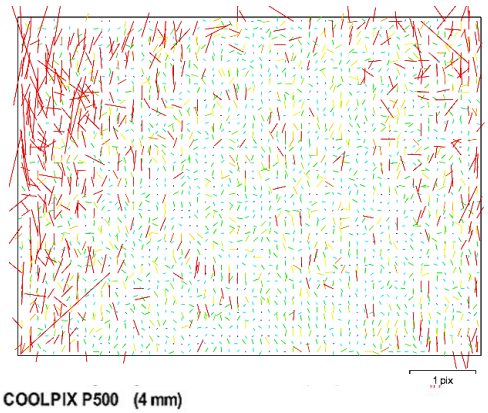


**COOLPIX P500 (4 mm)**
24 images

| Resolution | Focal Length | Pixel Size | Precalibrated |
|---|---|---|---|
| **3264 x 2448** | **4 mm** | **1.84 x 1.84 µm** | **Yes** |

| | | | |
|---|---|---|---|
| Type: | Frame | F: | 2212.1 |
| Cx: | -0.738526 | B1: | 4.02577 |
| Cy: | -4.36047 | B2: | 1.24004 |
| K1: | 0.0262943 | P1: | 5.40636e-05 |
| K2: | -0.0184442 | P2: | -0.000713147 |
| K3: | 0.0223008 | P3: | 0 |
| K4: | -0.026533 | P4: | 0 |

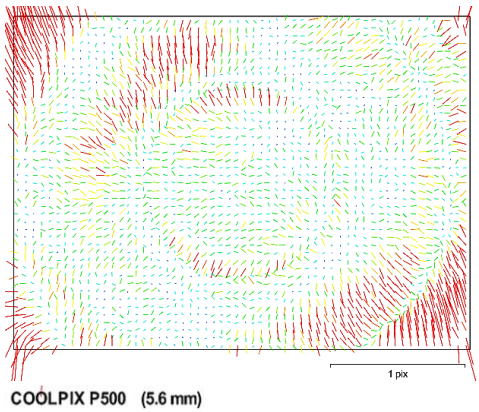


**COOLPIX P500 (5.6 mm)**
389 images

| Resolution | Focal Length | Pixel Size | Precalibrated |
|---|---|---|---|
| **3264 x 2448** | **5.6 mm** | **1.86 x 1.86 µm** | **Yes** |

| | | | |
|---|---|---|---|
| Type: | Frame | F: | 3171.5 |
| Cx: | -17.1344 | B1: | -0.735293 |
| Cy: | -29.2164 | B2: | 0.777399 |
| K1: | 0.00613356 | P1: | -0.0014471 |
| K2: | 0.162117 | P2: | -0.00298922 |
| K3: | -0.797936 | P3: | 0 |
| K4: | 1.00468 | P4: | 0 |

Figure 23. Image Residual Comparison PS1 & PS2

### 4.3.4. Combined Processing of Batch PS1 and PS2

Two individual processes were analyzed in Agisoft PhotoScan. Firstly, all the 479 images captured with the Nikon camera were processed altogether and then a separate process was performed for the PS1 and PS2 photosets.

The **processing of all 479 photos** altogether resulted in the alignment of 473 cameras; the reconstruction parameters were set to high quality and mild depth filtering. After a total of 12 hours and 22 minutes, the model rendered had an RMS reprojection error of 0.866 pixels, but a max reprojection error of 50.9621 pixels. The sparse point cloud from this alignment is shown in figure 24 below.

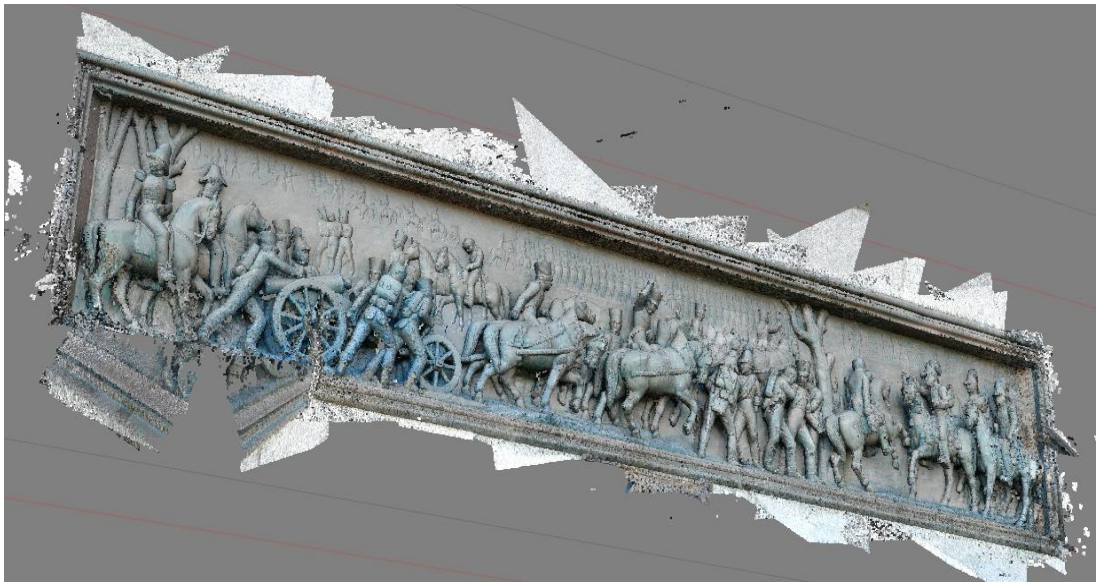

Figure 24. Sparse Point Cloud (Nikon Camera All Imagery)

As it can be clearly observed, the model presented a huge alignment issue on the lower left corner of the frame. This occurred because the images were aligned with respect to the camera settings at the time of the capture. That is 389 images with a fixed focal length and 79 photos with different focal lengths due to the automatic setting. The model also showed that these two batches presented different scales.

It can be noted that the camera calibration parameters generated by Agisoft Lens had to be manually included. This could have also caused the unalignment issue, probably because the software processed the photos from PS1 and PS2 with the same calibration parameters, when in reality although the photos were acquired with the same camera, one of the batches had automatic adjustment camera settings.

### 4.3.5. Separate Processing of Batch PS1 and PS2

In order to fix this issue a **separate process for the batches PS1 and PS2** was performed. For the new processing, a previously measured distance was included, as well as a number of manually selected tie points were placed in both batches separately. With this approach, the scale definition as well as the local reference system were intended to be established before trying a realignment process.

The reconstruction for the batch PS2 resulted in 389 aligned images. A partial model was rendered with high quality and moderate depth filtering parameters, which took 3 hours 53 minutes to be completed. The rendered mesh had an RMS reprojection error of 0.4605 pixels and a max reprojection error of 3.395 pixels. The reconstructed model is shown in figure 25 below.

Figure 25. Dense Point Cloud from Batch PS2

For the individual process of the PS1 batch, only 24 photos were carefully selected from the 78 images available in this batch, thus only focusing in the area that presented most of the missing information. The alignment resulted in 21 images being merged. A partial model was processed with high quality and mild depth filtering parameters, which only took 8 minutes. The rendered mesh had an RMS reprojection error of 0.606 pixels, and a max reprojection error of 16.057 pixels. The reconstructed model is shown in figure 26 below.

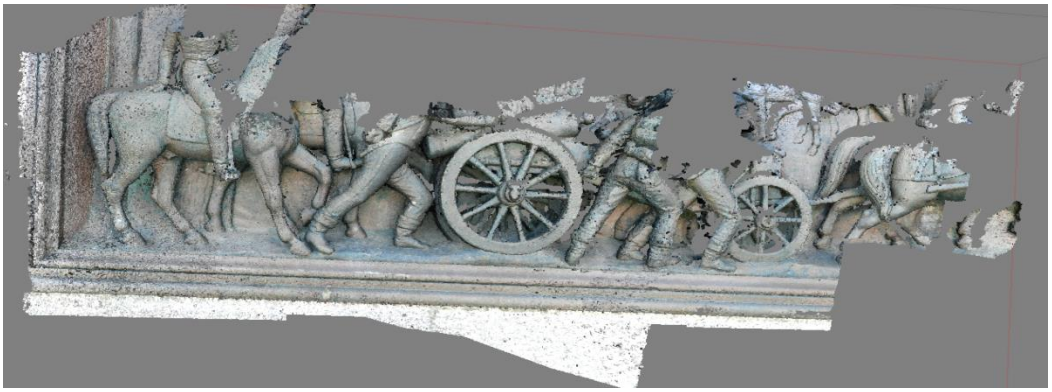

Figure 26. Dense Point Cloud Batch PS1 (Nikon Camera)

### 4.3.6. Merging of Components

The two chunks with 24 and 389 were realigned with the distance and markers constrains. Then a dense point clouds were merged, although the result was an unaligned model, created one on top of the other in the lower left corner of the frieze. This can be seen in figure 27 below.

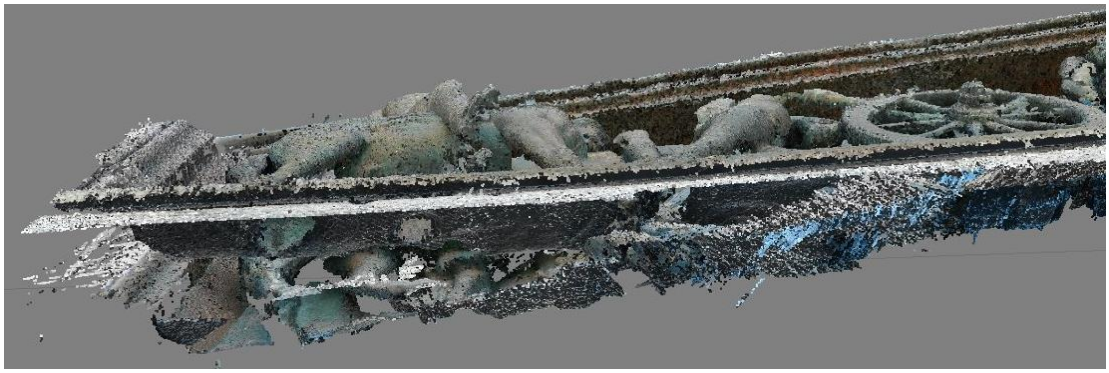

Figure 27. Sparse Point Cloud from Unaligned Batches PS1 and PS2 (Nikon Camera)

A different order was set and the realignment launched, that resulted in an optimal solution. The images were successfully aligned, merged, and then the dense point cloud was created. The result can be seen in figure 28 below.

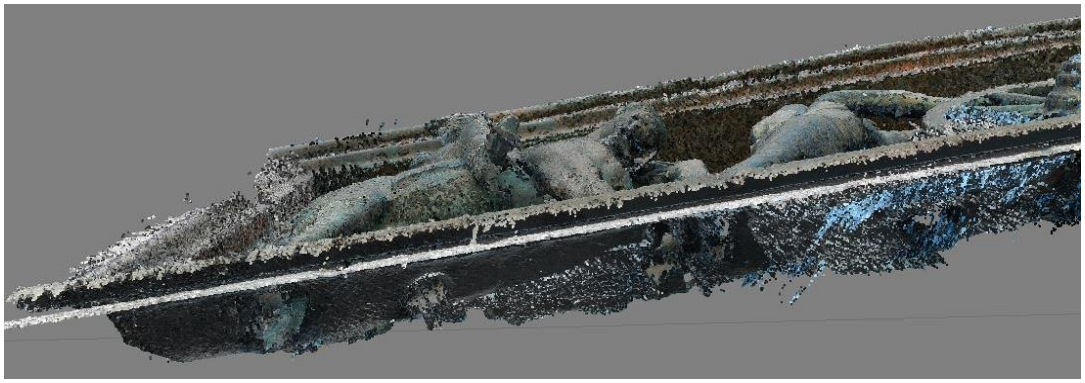

Figure 28. Sparse Point Cloud from Aligned Batches PS1 and PS2 (Nikon Camera)

### 4.3.7. Model Comparison

The software parameters were changed so as to perform a quality visual assessment and to achieve a high quality final product. The visual comparison is shown as follows in figures 29 through 32.

Figure 29. Meshed Model

Figure 30. Textured Model

Figure 31. Textured Generic Mosaic Color Correction

Figure 32. Textured: Adaptive Orthophoto, No Color Correction

## Process with color correction:

The color correction option (figure 33) allows balancing the brightness across all the images in the set before texturing and it doesn't depend on the blending mode used. For this last attempt the extra processing time was useful, since it provided a real and detailed high-resolution model.

Figure 33. Color Correction

### 4.3.8. CPR Results Overview

| | PS1 | PS1 & PS2 | PS1 | PS2 |
|---|---|---|---|---|
| Camera used | Sony | Combined | Nikon | Nikon |
| Input images | 126 | 479 | 24 | 401 |
| Aligned images | 126 | 473 | 21 | 389 |
| % of alignment | 100% | Alignment issue | | |
| Image overlap | 50% | | | 80% |
| Reconstruction Parameters | High quality and mild depth filtering | High quality and depth filtering | High quality and mild depth filtering | High quality and moderate depth filtering |
| RMS and max. reprojection error | 0.388 pixels | 0.866 pix – 50.9621 pix max. | 0.606 pix<br>- 16.057 pix max. | 0.4605 pix – 3.395 pix max. |
| ISO focal length | High; > 400 | < 200 | Close scene mode, mean focal length 4mm | 5.6mm |
| Accessories used | Tripod | | | Tripod |
| Total processing time | 59min | 12 h 22min | 8min | 3h 53min |

Table 4. CPR Results Overview

### 4.3.9. Final CRP 3D Model

Various settings with 6 Million points were tried out in order to achieve the best result possible, the visual comparison is shown as follows with figures 34 to 36.


Figure 34. Dense Point Cloud


Figure 35. Shaded, Textured - Generic, No Color Correction

Figure 36. Textured - Adaptive Orthophoto, No Color Correction

## 4.4. Combined CRP and TLS Data Processing

In the present section the combined data acquired from both surveying techniques will be processed in RealityCapture. This photogrammetric software is capable of processing both data sets simultaneously. For this exercise the methodology followed was basically the same as before, the first step is the data input, followed by the alignment of cameras that generates the sparse point cloud and the reconstruction process from which the dense point cloud is derived. The process finishes when texture and color are applied to the rendered model.

A total of 708 images and 10 individual scans were uploaded. These images correspond to the three photosets PS1, PS2 and PS3. Manual measurements were taken from this imagery, including specially the common black and white targets used for the TLS acquisition.

As a result of the alignment process, the scanned data and the imagery were merged into individual components. The sparse point cloud from the 639 aligned cameras is shown in figures 37 and 38 below. As it can be observed, the difference in focal length or the automatic camera adjustment did not represent a limit for this software to properly orient the cameras (seen in figure 37) as it had happened with PhotoScan. This software has the advantage that during the image registration it calculates the camera positions, orientations, and internal camera states for every input image individually. In other words, the automatic interior and exterior orientations are performed for each camera, thus allowing afterwards the automatic multi-image pairing. Nonetheless, the lower left part of the frame, like in Agisoft, still had some missing information.

Figure 37. Sparse Point Cloud From 639 Aligned Cameras

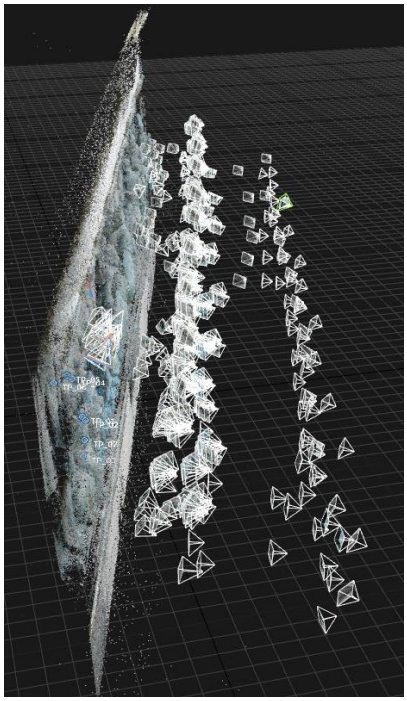

Figure 38. Camera Positioning and Alignment

Given that the PS3 dataset that included the targets was also added to the input files, some manual control points could be added assigning the same local coordinates extracted from the scanner point cloud. The GCP accuracy was intended to be at a subpixel level and not higher than 0.2 and for manually added tie points a maximum of half a pixel error was allowed, thus representing a weight difference for the different types of measurements. This is shown in figure 39 in the following page.

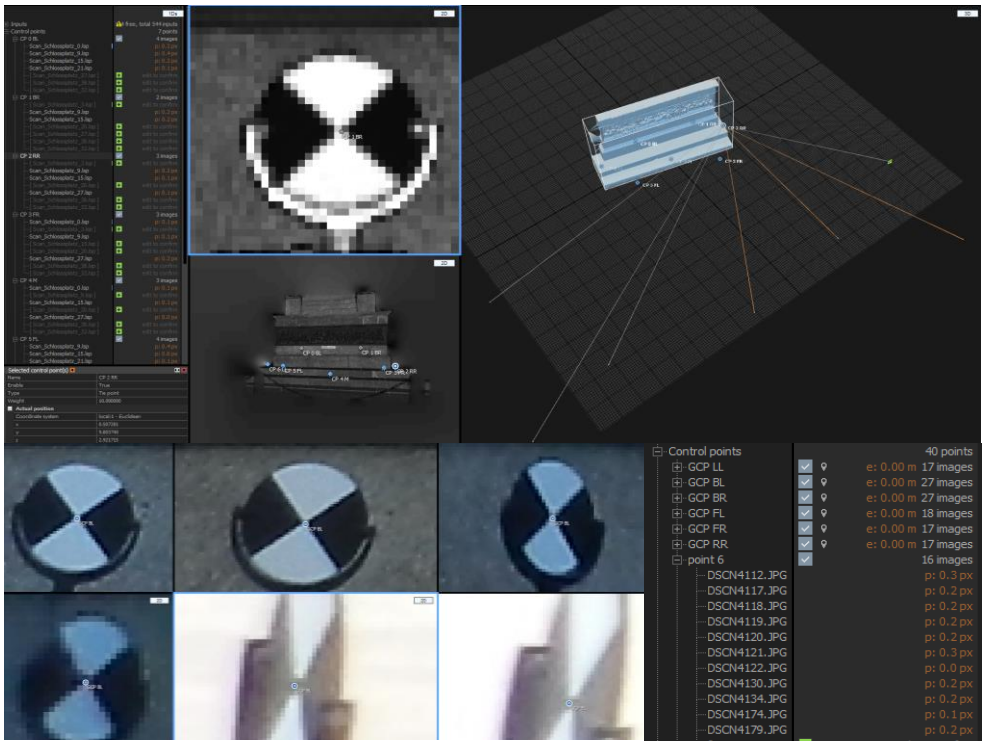


Figure 39. Tie Point and GCP Definition

A sample of the final alignment result is shown in figure 40 below. It can be seen how both sparse point clouds make use of the tie points and GCP defined for that purpose. The projecting rays from each point are referred to both the laser scanned and the individual camera positions.

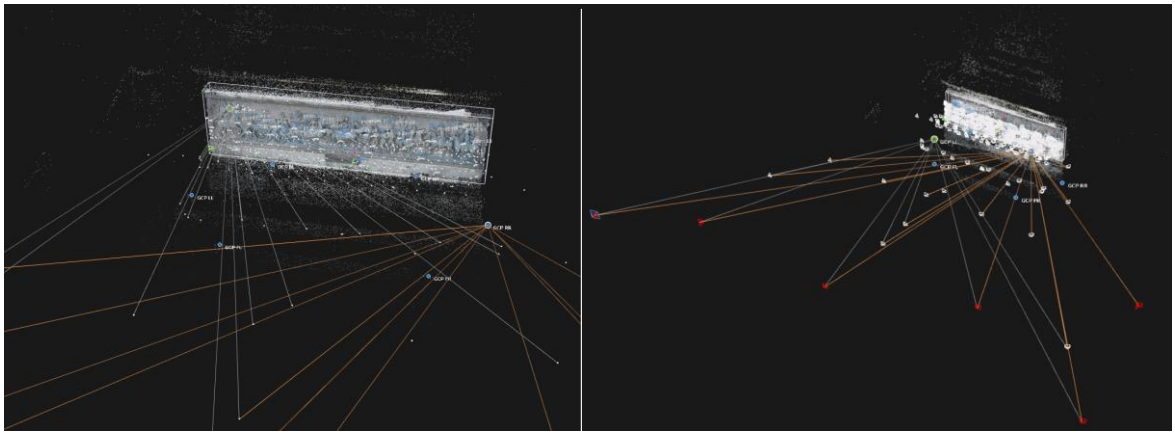

Figure 40. . Tie Point and GCP Final Alignment

As complementary information, the way that the specific laser scanner used for this exercise operates to record the point clouds, is shown in figure 41 to the right. It can be clearly seen that it captures from the middle at a 45° angle to both left and right.

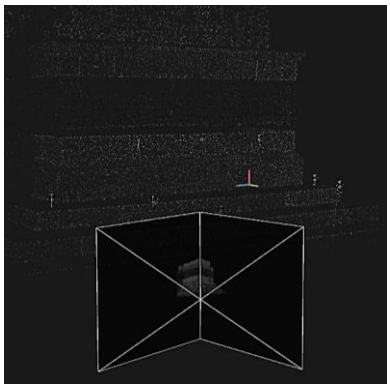

Figure 41. Laser Scanner Capture

In order to have a clear visual idea of the data acquired with the laser scanner, this was also rendered individually. As expected, the captured information had a homogeneous surface including occluded areas thanks to the oblique scanning positions and also areas beyond the frame; apart from having no colour information or clearly defined edges. All of these can be seen in figure 42.

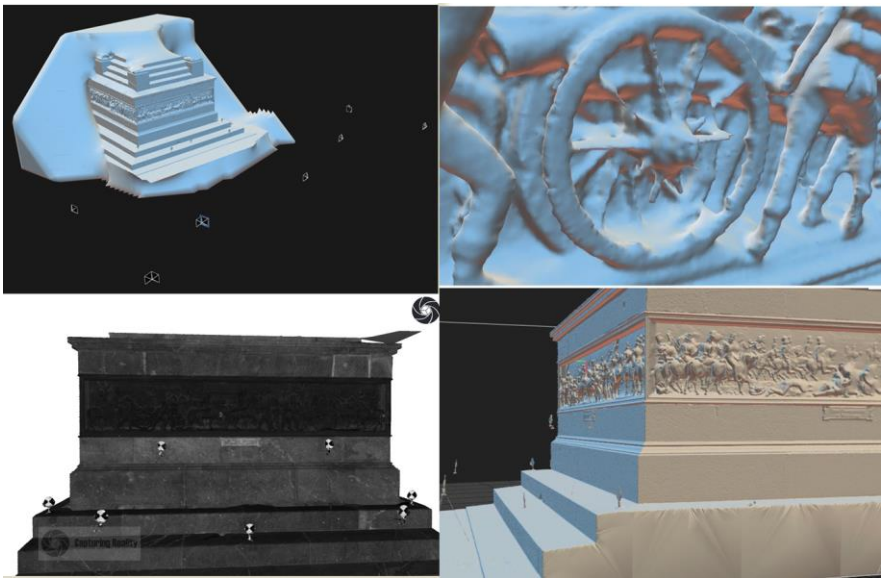

Figure 42. Laser Scanned Data Reconstruction

After assigning local coordinates in the same system to the target network, a number of tie point were manually selected in order to complement the color and texture information missing from the imagery. A sample is shown in figure 43. This also aimed to merge the photographs that were not initially aligned with the other 639, but had been aligned in individual batches. This is also visible in figure 43 as follows.

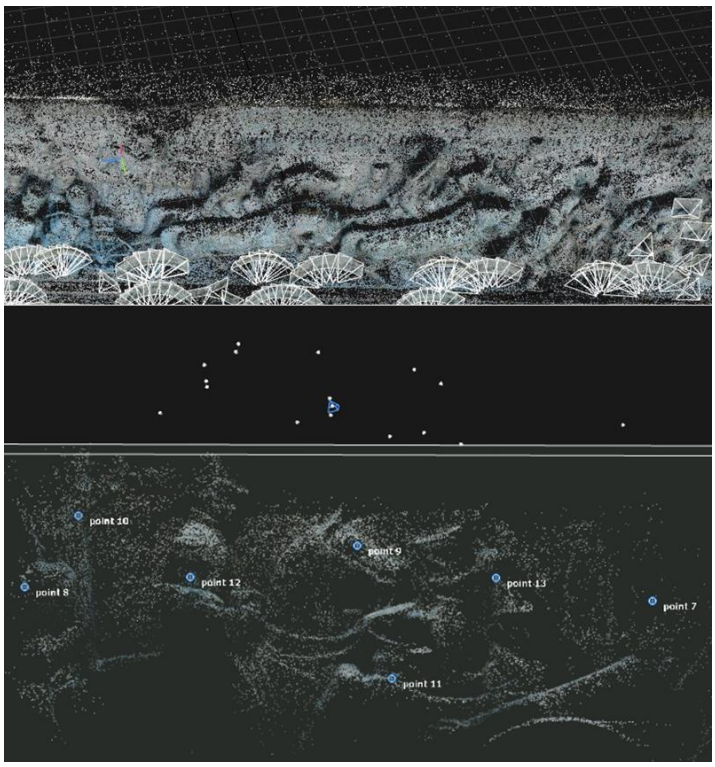


Figure 43. Missing Information and Tie Point Definition

The alignment process was launched again in order to merge the individual chunks obtained from the imagery and the laser scanned data. This process could now make use of the manually defined tie points and ground control points (GCP) assigned for the target network. The space point cloud of the successful merging procedure of individual components can be seen in the image to the right (figure 44) and the image below (figure 45). The latter clearly displays that the lower left side of the frame has now the information needed for its modeling. The reconstruction in normal detail was subsequently launched.

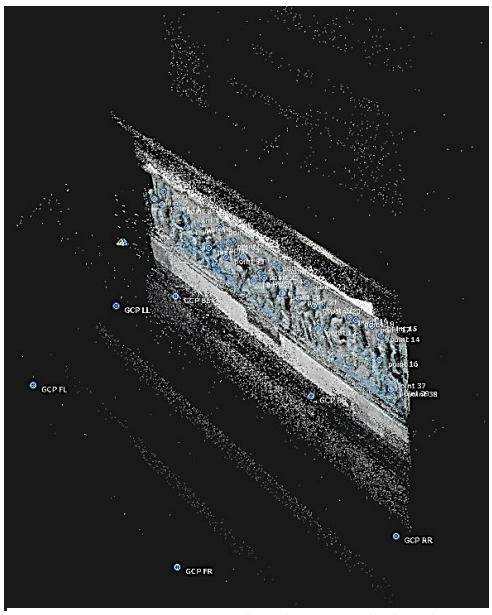


Figure 44. Space Point Cloud Merged Chunks

Figure 45. Enhanced Alignment CRP and TLS Merged Data

The next figure (46) shows a visual comparison of the different results in the reconstruction stage, with normal detail. It first displays the result obtained solely with laser scanned data, then the rendered result from part of the imagery and lastly the reconstruction with all the images merged and aligned after the tie point and GCP measurements. The dramatic increase in visual quality is evident.

Figure 46. Visual Comparison of Different Reconstruction Results

## 4.5. Final 3D Model reconstruction with CRP and TLS

To achieve an accurate digital photo-realistic surface model, various parameters were changed in the dense point cloud reconstruction. Samples of failed processes are shown below. The first figure 47 shows a superimposed frieze backwards and forward. The reason for this collapsed model was not entirely found out – the process was simply launched again with a different set of parameter. Given that RealityCapture is commercial software, the specific algorithms and procedures are not made public, even though the developers have an online help forum; it offered little help with this specific issue.

Figure 47. Superimposed Frieze

The second image (figure 48) shows a partially reconstructed dense point cloud made of 24 parts and approximately 44.3 million triangles (44277492 exactly). This high detailed reconstruction took over 7 hours of processing time and although it did not stop due to a software or hardware error, it is obvious that the result is utterly insufficient.

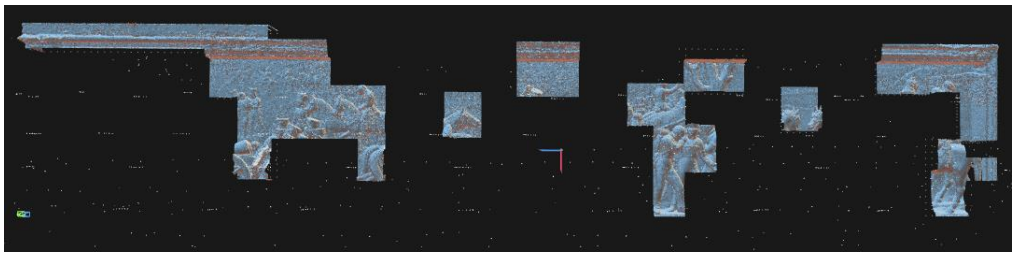

Figure 48. Partially Reconstructed Dense Point Cloud

The last example of a partially reconstructed dense point cloud is shown in figure 49. This model resulted in 42 parts and approximately 76.1 million triangles (76065174 exactly). This high detailed reconstruction took under 3 hours of processing time and the result was obviously insufficient. What is most interesting here is that precisely the missing information shown in the sparse point cloud of figure 45, was reconstructed here with no gaps, specifically both upper corners of the frame. The process was launched again only changing the definition from high to normal. The results are displayed in the following page.

Figure 49. Partially Reconstructed Model (High Quality)

A sample of the final 3D photorealistic model, reconstructed with all datasets PS1, PS2 and PS3, is shown as follows. This final model processed with RealityCapture included data from both surveying methodologies: CRP and TLS.

The intended generation of a visually compelling output resulted in a dense point cloud of homogeneous surface, which used a total of 685 images and 10 scanned data files (.lsp). A total count of 2138957 points constituted the sparse point cloud and approximately 6.9 million triangles (6918670 exactly) the dense point cloud. It presented a mean error of 0.336153 in pixels and resulted in a texture resolution of 8192 x 8192 with 72% texture utilization. This was due to the fact that only preselected high quality images were chosen for the texturing and coloring process. The reconstruction lasted just over 45 minutes in total. It needs to be noted that once the images and scan data were merged, the subsequent point clouds had both metric and locally referenced properties. The final model will be displayed in the next section.

The software offers the option to export accurate and high-resolution screenshots of the reconstructed object, one of which is shown below in figure 50 so as to closely inspect the quality of the 3D model before applying texture or color.


Figure 50. . CRP and TLS High Quality Resolution Samples

# PART V

## 5. Results

To recap, a final model was derived in Agisoft PhotoScan only from the imagery captured in the data sets PS1 and PS2. The latter applied the recommended photogrammetric planning instructions, whereas the other one was a used crowd-source approach capture with different cameras at different viewing angles and focal lengths. The final chosen result was a merged solution of the separate process of both batches. In order to perform a close visual assessment, only a sample of this result is shown in figures 51 through 54 in the next comparison section. The complete result can be found in the appendix section at the end of this document.

On the other hand the model obtained with the RealityCapture software used the combined input of data sets PS1, PS2 and PS3 plus the laser scanned data. The chosen final end-product was a merged solution of the CRP and TLS data batches. In order to achieve their final alignment, both GCP and tie points were used. For the reason already mentioned, only a sample of this result is shown in figures 51 through 54 in the next comparison section. The complete result can also be found in the appendix section at the end of this document.

## 5.1. Final Model Comparison and Quality Assessment

In order to perform a quantitative and a qualitative visual assessment, three final models will be presented in this section. The first 3D model (M1) corresponds to the final result rendered exclusively from imagery (PS1 and PS2) and processed in Agisoft PhotoScan. The second model (M2) is also a result obtained exclusively from all the imagery captured (PS1, PS2 and PS3) but processed with RealityCapture. This software was also used to render the third model (M3), which is the combination from all the data acquired through both surveying methods CPR and TLS. The table below (Table 5) shows a summary of the most important features of each rendered model.

| | M1 | M2 | M3 |
|---|---|---|---|
| Processing Software | PhotoScan | RealityCapture | RealityCapture |
| No. of Images aligned | 366/413 | 639/728 | 685/728 |
| Alignment Percentage | 88,62% | 87,77% | 94,09% |
| RMS Reprojection Error (pixels) | 0,4636 | 0,3369 | 0,3362 |
| Max Reprojection Error | 10,0626 | 1,6832 | 0,9999 |
| Software Settings | High Quality | Normal Quality* | Normal Quality* |
| Dense Point Count | 97.795.942 | 1.971.556 | 6.918.670 |
| Tie/GCP Used | 10 | 7 | 40 |
| Reference System | Local | None | Local |
| Metric Properties | True | False | True |
| Total Processing time | 1h 56m | 1h 50m | 48m |

Table 5. Final Model Feature Comparison

*RealityCapture has the option to choose form some lens distortion models for the alignment phase. The one selected to process both M2 and M3 models works for optics with less than 180° angle. It is a polynomial model of radial distortion with 3 modeling parameters, extended with tangential distortion to compensate the offset of lenses, although the current optics has a negligibly small tangential error. It also includes a skew and aspect ratio.

From the table above, it can be seen that the most accurate result out of the three models was achieved combining both CRP and TLS data (M3). Not only the overall alignment was improved, but also the total reconstruction time was practically halved. An important difference is the use of GCP and extensive tie points, which allowed the alignment of a lot more images and moreover it provided the model with precise metric properties and locally referenced coordinates. The last model also has the lowest mean and maximum reprojection error (RMS).

At the beginning of the project, in the planning phase, it was hypothesized that a more accurate and complete end-result would be obtained with the model reconstructed from the combined laser-scanned and photogrammetric datasets. It was anticipated that the model obtained only by the means of CRP would require further work, specifically due to the lack of precise metric qualities and/or direct coordinates. As an additional objective of the present work, the qualitative and quantitative analysis would be complemented in order to prove or disregard this assumption.

It is numerically evident from table 5 that the best result between the models that were reconstructed only from imagery is M2. In addition, given that the M2 and M3 models were created with the same software and under the same parameters, M2 it is considered as the base for M3 and thus it is left outside this specific visual analysis. Nonetheless, it will be considered in the cloud to cloud comparison in the corresponding section.

## 5.2. Visual Quality Comparison (Agisoft vs. RealityCapture)

The visual assessment considers only the 2 contrasting models, M1 and M3. These will be meticulous inspected with samples from each one. Due to space restrains the complete models are only given in the appendix section. Furthermore, by not considering M2 in the present analysis, an indirect software performance comparison is carried out. Underlined in blue are the samples acquired from the Agisoft PhotoScan (henceforth AP) that rendered only a photogrammetric solution, and underlined in red are the samples of combined CRP and TLS data obtained with RealityCapture (henceforth RC).

### Sample 1: Top View Scenes

There are some noticeable visual differences between the final models rendered by the two software used. Some of which will be explained in the following paragraphs.

Figure 51. Sample 1A – Top View Scenes

As shown in figure 52 below, both photogrammetric software performed effectively especially in the sharp definition of the kepis' edges (or war caps) and animal figures. The visible poor performance on the left horse limb can be attributed to the lack of information in the imagery captured for this occluded area, although RC had a smoother delineation compared to AP.

In figure 51A in the previous page AP accomplished a better result than RC. This degraded result may have been caused due to the lack of tie points in RC to aid merge the images that were left outside the alignment because of their high changes in perspective; as a consequence the dense point cloud was left incomplete.

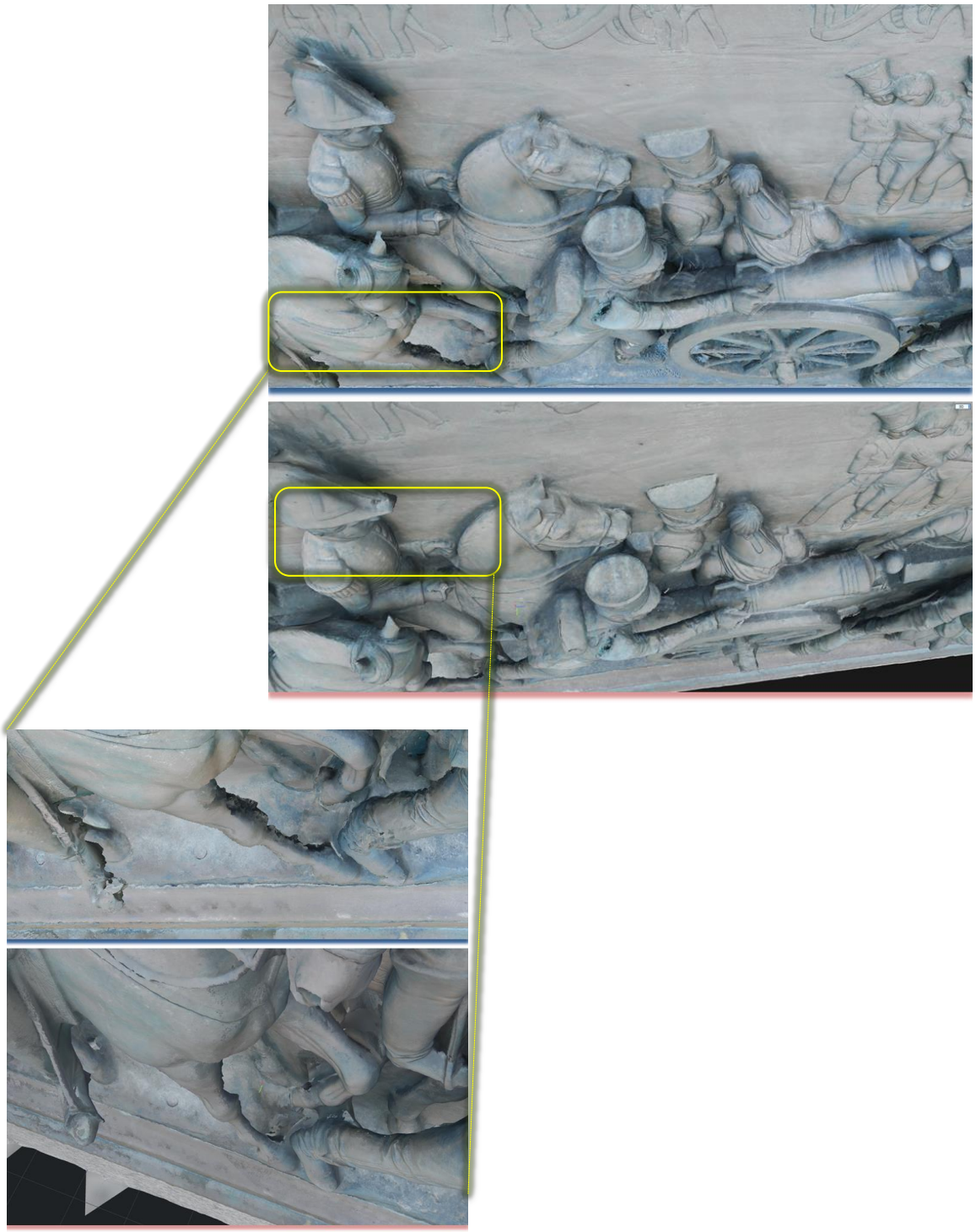

Figure 52. Sample 1B Top View Scenes

## Sample 2: Front Scene

The tainted blue color that is portrayed in the AS model, makes it look less sharp compared to RC model (figure 53). On the other hand, although the upper frame seems to be better rendered in AS it does not show a horizontal alignment, as it is visible for the result with RC, which portrays a rather poor reconstruction for this upper side of the frame.

Figure 53. Sample 2 Front Scene

## Sample 3: Bottom View Extract

The continuous surfaces can be seen of the lower parts throughout both models. Although less defined edges and unattached elements were reconstructed in some parts of the AP model (figure 54).

Figure 54. Sample 3 Bottom View Extract

In conclusion, RC showed a better performance in texturing, colorising and reconstructing the dense point cloud of the 3D model.

## 5.3. Cloud to Cloud Comparison (CloudCompare)

The generated dense point clouds from the three models M1 M2, M3 will be compared and discussed as follows. The CloudCompare software aids in the computation of the cloud to cloud distance. The model including the photogrammetric and laser scanned data (M3) was set as a reference since, as it was seen from the quantitative and visual assessment, it had the best accuracy and overall completeness. The maximal distance was set to 0.25 (due to computational restrictions). To be able to distinguish the clear differences, the reference cloud from M3 is displayed in RGB colors, whereas the cloud that is being compared (M1 or M2) is displayed as a color-coded distance difference to the reference cloud.

The first image (Figure 55) shows that between both dense point clouds acquired in RC, M2 and M3, the biggest dissimilarity reaches the upper threshold limit of 0.25 in specific small areas like the upper left side of the frame or some relief figure parts in the right (a shoulder and a foot). Most of the distance difference between dense point clouds does not overpass the value of 0.031 setting the mean difference below 0.015.

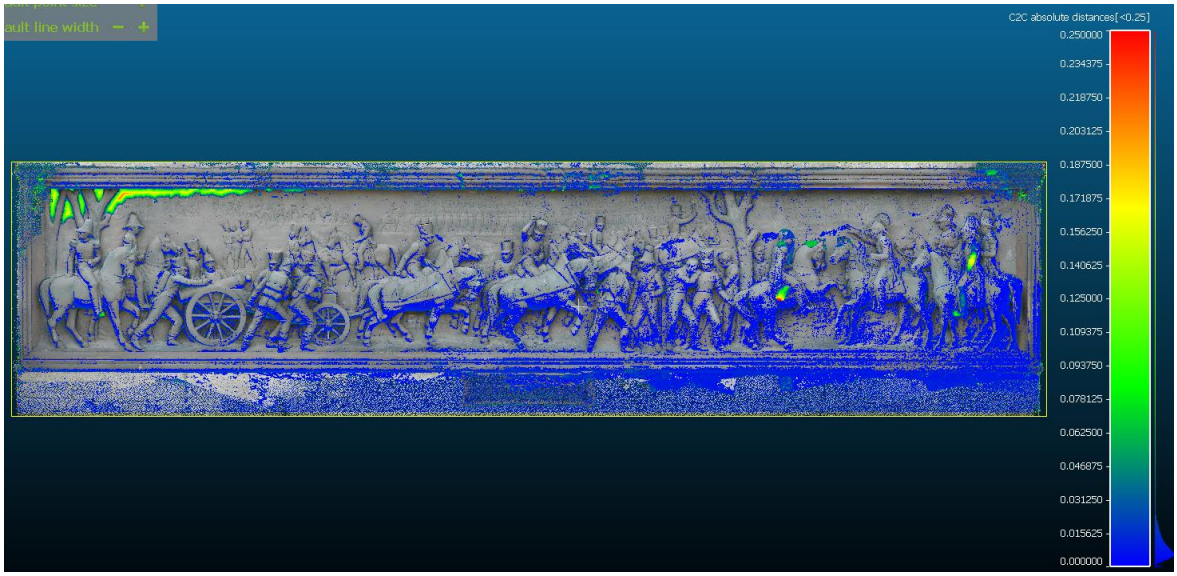


Figure 55. Cloud Comparison M2 vs M3

On the other hand, figure 56 shows the difference between both dense point clouds, M1 and M3. The biggest dissimilarity that reaches the upper threshold limit of 0.25 is outside of the frame and thus not considered as important. In the middle of the dense cloud of the frieze there is a concentration of points whose highest distance difference does not overpass 0.062 setting the mean difference just below 0.015. However, at a closer examination, it was found out that the alignment of these two clouds was not exact (shown in figure 56), even though a fine registration was executed. It is assumed that the reason for this occurrence is the adoption of different scales by each model. In other words, M3 derived the scale precise from the laser-scanned data, whereas M1 had a manually measured and specified scale. A close-up of this unalignment issue is revealed in figure 57. For this reason a higher vale for the distance difference was used.

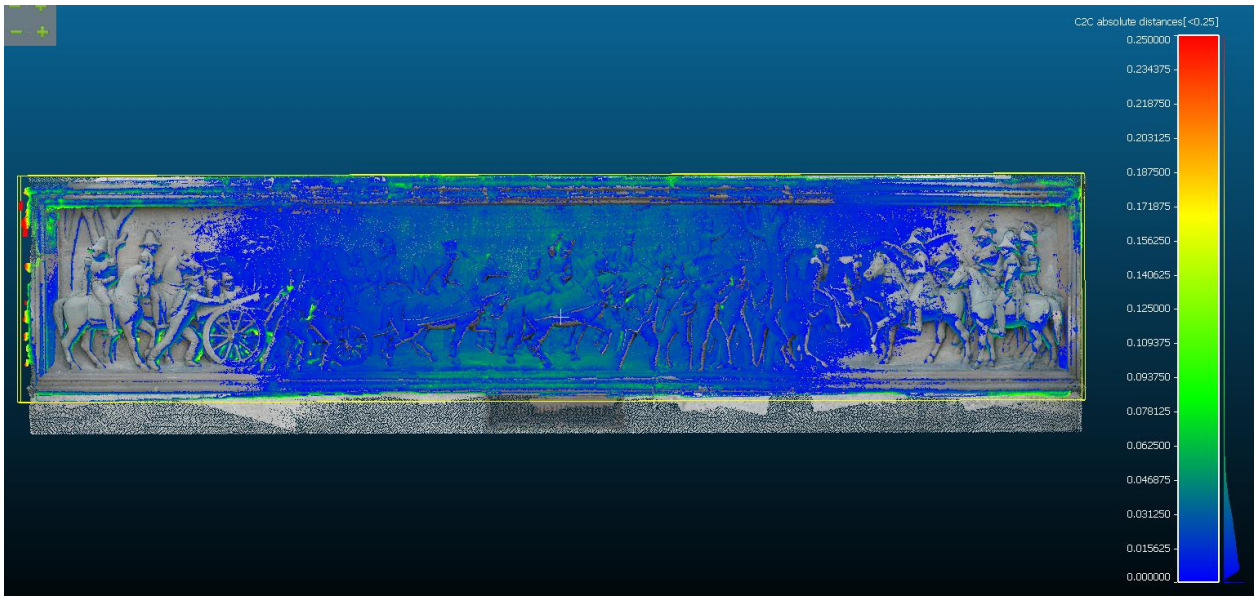


Figure 56. Cloud Comparison M1 vs M3

Image 65 shows the difference between dense point clouds M1 and M3, but doubled the highest threshold limit of 0.55. Some dissimilarity is shown in specific small areas throughout the frieze in some relief figure parts such as shoulder, feet or especially linear elements. For this reason, a higher vale for the distance difference was used.

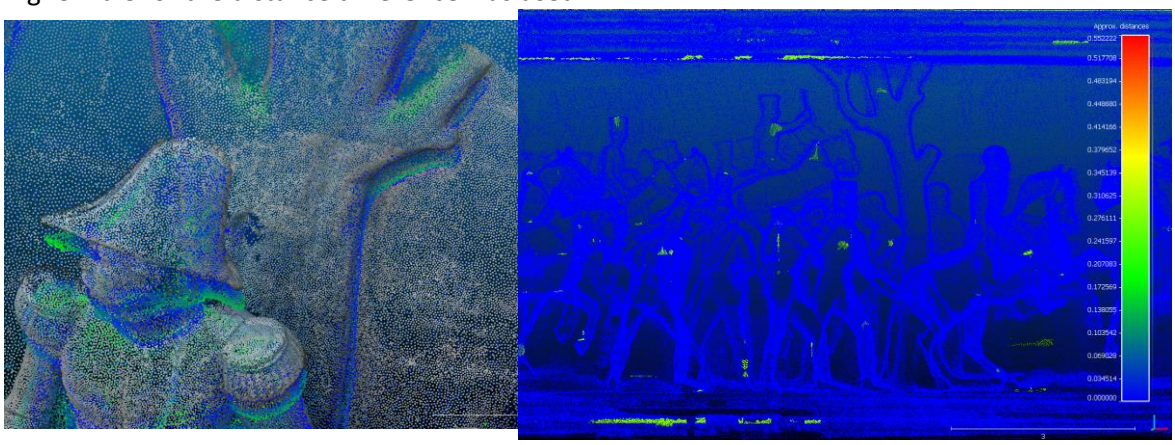

Figure 57. Cloud Misalignment and Distance M1 vs M3

Figure 58, acquired from the Agisoft PhotoScan report shows the image overlap and camera locations of the M1 model. As previously shown, more information is needed along the frame for it to be properly reconstructed.

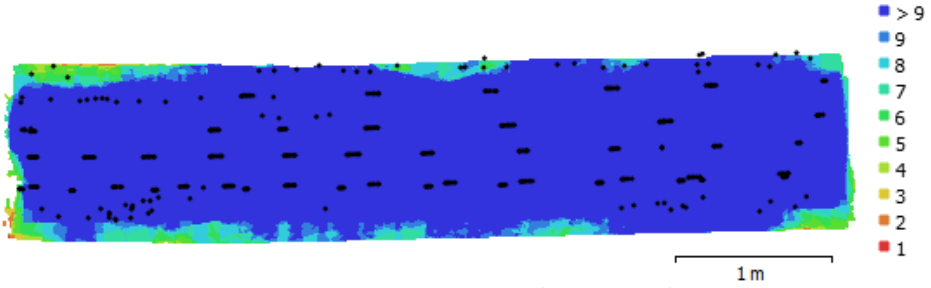


Figure 58. Camera Locations And Image Overlap

# 6. Budget

| Expenses | Workforce | Annual Costs | Daily Costs | Hourly Costs | Duration | Total |
|---|---|---|---|---|---|---|
| **Field Observation** | | | *wordays | | | |
| Salary* | 1 Engineer | 30,360.94 € | 121.44 € | 15.18 € | 5h | 75.90 € |
| | 1 aide | 24,538.64 € | 98.15 € | 12.27 € | 3h | 36.81 € |
| Transport | 1 Engineer | 8,760.00 € | 24.33 € | | 1d | 24.33 € |
| | 1 aide | 8,760.00 € | 24.33 € | | 1d | 24.33 € |
| Workstation Purchase (Laptop) | | 2,300.00 € | 6.30 € | | 14d | 88.22 € |
| Scanner rental* | | 109,135.00 € | 436.54 € | | 1d | 436.54 € |
| Photogrammetric camera Rental* | | 3,128.57 € | 12.51 € | 1.56 € | 4h | 6.26 € |
| Tripod Rental* | | 3,826.76 € | 15.31 € | 1.91 € | 4h | 7.65 € |
| **Data Processing** | | | | | | |
| License Agisoft Photoscan* | | 3,349.00 € | 13.40 € | 1.67 € | 8d | 107.17 € |
| License Reality Capture* | | 2,490.00 € | 9.96 € | 1.25 € | 8d | 79.68 € |
| Donation Cloud Compare* | | 1,200.00 € | 4.80 € | 0.60 € | 5d | 24.00 € |
| License Leica Cyclon * | | 13,920.00 € | 55.68 € | 6.96 € | 1d | 55.68 € |
| Salary* | 1 Engineer | 30,360.94 € | 121.44 € | 15.18 € | 8d | 971.55 € |
| **Total Before Taxes** | | | | | | 1,938.12 € |
| IVA (21%) | | | | | | 407.01 € |
| Industrial Benefit (25%) | | | | | | 484.53 € |
| **Total After Taxes** | | | | | | 2,829.66 € |

Table 6. Planned Budget

The budget has been based on the annual salary obtained from the official published document for Spain. An extract of which is shown below.

| CATEGORIA | NIVEL | SALARIO AÑO | OBSERVACIONES |
|---|---|---|---|
| Ingeniero Superior/Licenciado | Máximo | 45.074,88 | Las cantidades que se reflejan en la presente Tabla se entienden globales por todos los conceptos, incluyendo el Complemento de Puesto y Mayor Dedicación. |
| | Mínimo | 31.222,24 | |
| Ing. Técnico/Titulado Grado Medio | Máximo | 40.768,36 | |
| | Mínimo | 30.360,94 | |
| Analista | Máximo | 38.184,44 | |
| | Mínimo | 27.733,97 | |
| Programador | Máximo | 34.667,44 | |
| | Mínimo | 24.274,41 | |
| Ingeniero/Licenciado (Junior) | 2º Año | 24.892,00 | A esta categoria le corresponden todos los conceptos salariales que estan marcados en el convenio |
| | 1º Año | 22.860,00 | |

Figure 59. Convened Salary 2016, Table A

| CATEGORIA | NIVEL | SUELDO BASE | PLUS CONVENIO | COMPL. EMPRESA | SALARIO DIA | SALARIO MES | SALARIO AÑO |
|---|---|---|---|---|---|---|---|
| Operador | A | 644,10 | 696,54 | 856,92 | 73,25 | 2.197,56 | 30.765,84 |
| Operador | B | 644,10 | 696,54 | 799,60 | 71,34 | 2.140,24 | 29.963,31 |
| Operador | C | 644,10 | 696,54 | 768,06 | 70,29 | 2.108,70 | 29.521,82 |
| Operador | D | 644,10 | 696,54 | 706,22 | 68,23 | 2.046,86 | 28.656,05 |
| Codificador | A | 614,46 | 635,42 | 663,51 | 63,78 | 1.913,39 | 26.787,42 |
| Codificador | B | 614,46 | 635,42 | 636,08 | 62,87 | 1.885,95 | 26.403,37 |
| Grabador de Datos | A | 584,23 | 609,89 | 467,94 | 55,40 | 1.662,05 | 23.268,70 |
| Grabador de Datos | B | 584,23 | 609,89 | 301,51 | 49,85 | 1.495,63 | 20.938,77 |

Figure 60. Convened Salary 2016, Table B

# 7. Conclusions

- Within the geoscience applications, a photogrammetry-based academic exercise that presented many difficulties during processing resulted in an accurate, high-resolution locally-referenced, photo-realistic 3D model, thanks to the theoretical foundation acquired beforehand.
- The best end-product was acquired by combining two important surveying techniques, close-range photogrammetry and laser scanning. This was proven after the quantitative and qualitative analysis of each derived model.
- The two approaches used to capture the images, photogrammetric and crowd-source input, have pros and cons. However, in this case the implementation of both resulted in a very detailed, high-resolution result.
- Now that many of the automated 3D modeling hurdles have been solved, only the issue of efficient image matching as effortlessly as human observers is left unsolved.
- The usage of amateur imagery in 3D model reconstruction makes sufficient photogrammetric knowledge a key issue in resolving every issue that arises during the object modeling procedure. In other words, it shifts the challenge to the skills of the designer.
- Some photogrammetric recommendations for the image acquisition must be taken into account on order to recreate a virtual realistic 3D model. A case in point is the low change in perspective and big overlaps with which the images need to be captured.
- A combined approach in the image acquisition phase proved that even though few images had to be disregarded due to radiometric or geometric deficiencies, the usage of photographs with a variety of viewing angles, focal lengths, scene modes and alike, did not represent a restrain for a successful aesthetic and photorealistic 3D model reconstruction. This is possible only when the algorithms implemented within the software operate in such way that allows a successful alignment of imagery with varied characteristics. In other words, the fact that RealityCapture computes the interior and exterior orientations for every image individually allows a more efficient automatic multi-image pairing than the obtained from Agisoft PhotoScan. The latter implements the same camera calibration parameters for all images of the same dataset and generated an unaligned sparse point cloud within the same dataset containing non-homogeneous imagery.
- Regarding texture generation, the increased brightness captured on the imagery does not limit the quality of the final high-resolution 3D model, provided that the software allows the pre-selection of acceptable images for this purpose and those images with non-truthful color can be deactivated at that stage, even though their geometric data has been already used for the alignment process.
- The usage of the tripod had a minor difference in the quality of the photos, although without it the equidistant spacing between stations and to the frieze would have been more difficult to monitor.
- The ISO and selection did not produce a high amount of noise that would damage the results of the 3D final model. The contrary was true for those images capture with a non-truthful bluish color.
- The modeling process with Photoscan presented more limitations and processing times than the equivalent acquired with RealityCapture.
- The present study shows that the 3D models with the highest number of points or which had taken the longest reconstruction time had by far the best quality.

- From a personal point of view, great knowledge was acquired not only in field work, but also in project planning and processing.
- A properly processed metric and photo-realistic end-product enables the user to derive accurate measurements without a direct contact to the frieze.
- From a cultural heritage point of view, the monument can be preserved, documented, accessed remotely and long distance through a truthful 3D digital model. This serves as a real metric reference of the real object from which an identic copy could be reconstructed.
- The object documentation will serve goals of different nature. Firstly, serving national heritage interests, this historic memorial will be preserved and in case of destruction, the exact replica can be reproduced. In the scientific sphere, the virtual model can be analyzed and/or evaluated. Given that the accurate measurements of the original model will be safeguarded, not only the comparison of sculpturing technics used at the time construction can be made, along with some theories, but also the methodology used to create the 3D model can be studied and improved even long distance. In the academic domain, the 3D reconstruction could be accessed from schools and libraries in order to offer a visually compelling model to enhance the learning of historic events. Photorealistic 3D models can be integrated into virtual environments and used in applications such as navigation tourism environmental and of course cultural heritage.

# References


*Benefits DSLR Portraits* . (2019). Retrieved July 2019, from Nikonusa: https://www.nikonusa.com/en/learn-and-explore/a/tips-and-techniques/benefits-of-taking-portraits-with-a-dslr.html

Balsa-Barreiro, J., & Fritsch, D. (2018). Generation of visually aesthetic and detailed 3D models of historical cities by using laser scanning and digital photogrammetry. *Digital Applications in Archaeology and Cultural Heritage, 8*, 57 - 64.

Briese, C. &. (2003). *Laserscanning and photogrammetry for the modelling of the statue Marc Anton.* Retrieved from ResearchGate: https://www.researchgate.net/publication/228910642_Laserscanning_and_photogrammetry_for_the_modelling_of_the_statue_Marc_Anton

Caradonna, G., Tarantino, E., Scaioni, M., & Figorito, B. (n.d.). Multi-image 3D Reconstrucion: A Photogrammetric and Structure from Motion Comparative Analysis. *DICATECh*, 306 - 318.

Cramer, M. (2017, November). Lectures Notes, Introduction-to-Photogrammetry.

Fau, M., Cornette, R., & Houssaye, A. (2016). Photogrammetry for 3D digitizing bones of mounted skeletons: Potential and limits. *Comptes Rendus Palevol, 15*, 968–977.

Fritsch, D., Khosravani, A., Cefalu, A., & Wenzel, K. (2011). Multi-Sensors and Multiray Reconstruction for Digital Preservation. *Wichmann, Week 11*, 305 - 324.

Geosystems, L. (2011). *Leica Geosystems*. Retrieved 03 16, 2019, from Leyca: https://w3.leica-geosystems.com/downloads123/hds/hds/HDS7000/brochures-datasheet/HDS7000_DAT_en.pdf

Gisresources. (n.d.). *Introduction to Photogrammetry.* Retrieved 6 19, 2019, from www.gisresources.com: http://www.gisresources.com/wp-content/uploads/2013/11/Introduction-to-Photogrammetry-LPS.pdf

Hartman, P. (2019). *PelserHartman 3D Measuring Solutions* . Retrieved August 2019, from https://www.meet-tekenwerk.nl: https://www.meet-tekenwerk.nl/wp-content/uploads/2013/04/Leica-HDS7000-pelserhartman.jpg

Hartmann, W., Havlena, M., & Schindler, K. (2016). Recent developments in large-scale tie-point matching. *ISPRS Journal of Photogrammetry and Remote Sensing*(115), 47 - 62.

Heipke, C. &. (2016, 03). Theme issue “State-of-the-art in photogrammetry, remote sensing and spatial information science”. *ISPRS Journal of Photogrammetry and Remote Sensing, 115*(006), 1-2.

Leica. (n.d.). *Meet Tekenwerk*. Retrieved 01 4, 2019, from https://www.meet-tekenwerk.nl/wp-content/uploads/2013/04/Leica-HDS7000-pelserhartman.jpg

Lerma, J., Navarro, S., Cabrelles, M., & Villaverde, V. (2010). Terrestrial laser scanning and close range photogrammetry for 3D archaeological documentation: the Upper Palaeolithic Cave of Parpalló as a case study. *Journal of Archaeological Science, 37*, 499 - 507.

Linder, W. (2006). *Digital Photogrammetry: A Practical Course.* Düsseldorf: Springer.

Luhmann, T., Maas, H.-G., & Fraser, C. (2016, 11). Sensor modelling and camera calibration for close-range photogrammetry. *115*, 37–46.

Luhmann, T., Robson, S., Kyle, S., & Hardley, I. (2006). *Close Range Photogrammetry.* Caithness, Scottland: Whittles Publishing.

Mayer, I., Scheiblauer, C., & Mayer, A. (2011). Virtual texturing in the documentation of cultural heritage -The domitilia catacomb in Rome. 1 -8.

Nikon. (n.d.). *COOLPIX P500* . Retrieved 01 4, 2019, from https://www.nikon.de/de_DE/product/discontinued/digital-cameras/2012/coolpix-p500

Remondino, F., Spera, M., Nocerino, E., Menna, F., & Nex, F. (2013). Dense image matching: comparisons and analyses., *October.* Milano.

Rodríguez-Gonzálvez, P., Rodríguez-Martín, M., Ramos, L. F., & González-Aguilera, D. (2017). 3D reconstruction methods and quality assessment for visual inspeciton. *Automation in Construction*, 49-58.

Schenk, T. (2005). *Introduction to Photogrammetry.* Ohio: Department of Civil and Environmental Engineering and Geodetic Science.

Sony. (n.d.). *Alfa 7II*. Retrieved 01 4, 2019, from https://www.sony.com/electronics/interchangeable-lens-cameras/ilce-7m2-body-kit

Wenzel, K. &. (2013). Image Acquisition and Model Selection for Multi-View Stereo. *International Archives of the Photogrammetry, Remote Sensing and Spatial Information Sciences, XL-5*(W1), 251-258.

Wenzel, K., Abdel-Wahab, M., & Ce, A. (n.d.). A Multi-Camera System For Efficient Point Cloud Recording n Close Range Applications. *Institute for Photogrammetry*, 1 - 6.

Westoby, M., Brasington, J., Glasser, N., Hambrey, M., & Reynolds, J. (2012). 'Structure from Motion' photogrammetry: A low-cost, effective tool for geoscience applications. *Geomorphology, 179*, 300 - 314.

Williamson, J. R. (2009, January 09). *Close-Range Photogrammetry*. Retrieved 06 2019, from Geospatialworld : https://www.geospatialworld.net/article/close-range-photogrammetry/

Wolf, P., Dewitt, B., & Wilkinson, B. (2014). *Elements of Photogrammetry with Applications in GIS.* NY: McGraw Hill Education.

Yang, R., Meng, X., Yao, Y., Chen, B., You, Y., & Xiang, Z. (2018). An analytical approach to evaluate point cloud registration error utilizing targets. *ISPRS Journal of Photogrammetry and Remote Sensing, 143*, 48 - 56.

## Appendix

### A. Final Photogrammetric Result (CRP, Agisoft)

### B. Final Result from the Combined Surveying Techniques (CRP and LS, RealityCapture)

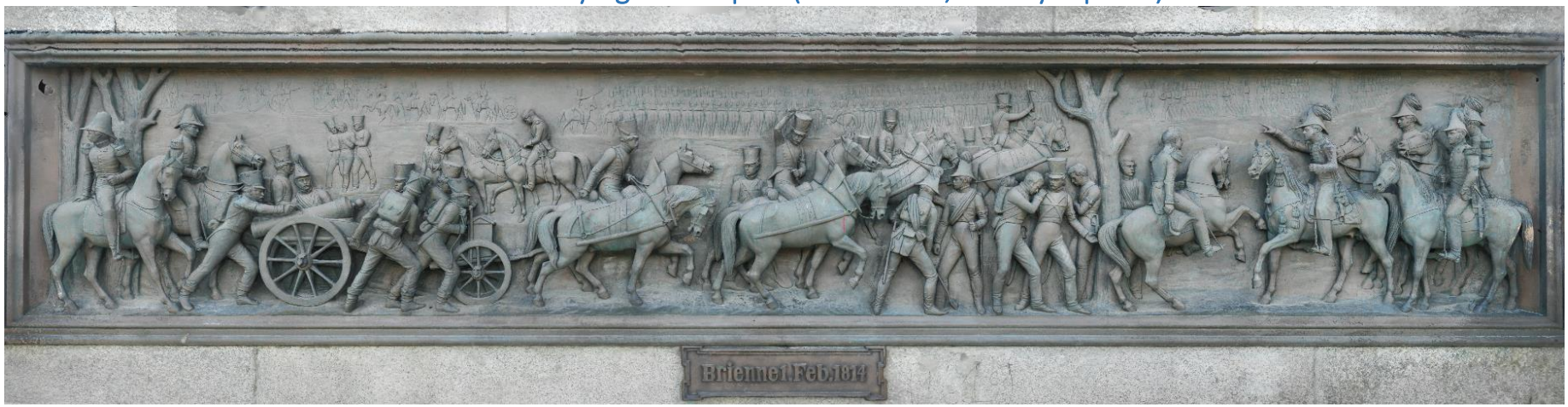

## C. Complete Agisoft Reports

Brienne 6mill texture generic color correction

| Property | Value |
|---|---|
| **General** | |
| Cameras | 413 |
| Aligned cameras | 366 |
| Markers | 10 |
| Scale bars | 2 |
| Coordinate system | Local Coordinates (m) |
| Rotation angles | Yaw, Pitch, Roll |
| **Point Cloud** | |
| Points | 1,062,204 of 1,653,182 |
| RMS reprojection error | 0.456767 (0.463609 pix) |
| Max reprojection error | 10.0626 (16.0568 pix) |
| Mean key point size | 0.0673725 pix |
| Effective overlap | 2.9659 |
| **Dense Point Cloud** | |
| Points | 97,795,942 |
| **Reconstruction parameters** | |
| Quality | High |
| **Model** | |
| Faces | 6,523,014 |
| Vertices | 3,267,243 |
| Texture | 16,384 x 16,384, uint8 |
| **Reconstruction parameters** | |
| Surface type | Arbitrary |
| Source data | Dense |
| Interpolation | Enabled |
| Quality | High |
| Face count | 6,523,015 |
| Processing time | 1 hours 38 minutes |
| **Texturing parameters** | |
| Mapping mode | Generic |
| Blending mode | Mosaic |
| Texture size | 16,384 x 16,384 |
| Enable color correction | Yes |
| Enable hole filling | Yes |
| UV mapping time | 2 minutes 1 seconds |
| Blending time | 16 minutes 11 seconds |

| | | | | |
|---|---|---|---|---|
| **General** | | | | |
| Cameras | 475 | 332 | 389 | 24 |
| Aligned cameras | 473 | 330 | 345 | 21 |
| Coordinate system | Local Coordinates (m) | 3 Markers<br>Local Coordinates (m) | Local Coordinates (m) | 3<br>Local Coordinates (m) |
| **Point Cloud** | | | | |
| Points | 138,227 of 471,728 | 161,259 of 340,926 | 1,041,506 of 1,628,745 | 20,698 of 24,437 |
| RMS reprojection error | 0.203104 (0.865889 pix) | 0.179267 (0.705383 pix) | 0.460537 (3.39536 max) | 0.137567 (0.606008 pix) |
| Max reprojection error | 1.41818 (50.9621 pix) | 0.539633 (23.4517 pix) | | 0.80073 (16.0568 pix) |
| Mean key point size | 3.76981 pix | 3.71591 pix | | 3.72709 pix |
| Effective overlap | 4.10467 | 3.94125 | 2.97399 | 2.42653 |
| **Alignment parameters** | | | | |
| Accuracy | High | High | High | Highest |
| Pair preselection | Disabled | Disabled | Generic | Disabled |
| Key point limit | 40,000 | 40,000 | 40,000 | 40,000 |
| Tie point limit | 4,000 | 4,000 | | 4,000 |
| Constrain features by mask | No | No | No | No |
| Adaptive camera model fitting | Yes | Yes | | Yes |
| Matching time | 7 hours 58 minutes | 3 hours 47 minutes | 2 hours 2 minutes | 1 minutes 43 seconds |
| Alignment time | 6 minutes 6 seconds | 2 minutes 38 seconds | 23 minutes 2 seconds | 2 seconds |
| **Optimization parameters** | | | | |
| Parameters | f, b1, b2, cx, cy, k1-k4, p1-p4 | | | f, b1, b2, cx, cy, k1-k4, p1, p2 |
| Optimization time | 7 seconds | | | 0 seconds |
| **Dense Point Cloud** | | | | |
| Points | 90,572,511 | 90,250,725 | 88,626,685 | 9,575,159 |
| **Reconstruction parameters** | | | | |
| Quality | High | High | High | High |
| Depth filtering | Mild | Mild | Moderate | Mild |
| Depth maps generation time | 3 hours 21 minutes | 3 hours 9 minutes | | 3 minutes 35 seconds |
| Dense cloud generation time | 58 minutes 13 seconds | 26 minutes 10 seconds | 1 hours 28 minutes | 23 seconds |
| **Model** | | | | |
| Faces | 86,126 | | | |
| Vertices | 43,224 | | | |
| Texture | 4,096 x 4,096, uint8 | | | |
| **Reconstruction parameters** | | | | |
| Surface type | Arbitrary | | | |
| Source data | Sparse | | | |
| Interpolation | Enabled | | | |
| Geometry type | Point cloud | | | |
| Face count | 90,000 | | | |
| Processing time | 3 seconds | | | |
| **Texturing parameters** | | | | |
| Mapping mode | Generic | | | |
| Blending mode | Mosaic | | | |
| Texture size | 4,096 x 4,096 | | | |
| Enable color correction | No | | | |
| Enable hole filling | Yes | | | |
| UV mapping time | 34 seconds | | | |
| Blending time | 1 minutes 17 seconds | | | |

# y3129424:TFG_Paola_Avila_Ebron.pdf

*por* Ginna Paola Avila Forero

---

**Fecha de entrega:** 06-sep-2019 07:15p.m. (UTC+0200)

**Identificador de la entrega:** 1168288688

**Nombre del archivo:** s_4333708f-0642-4e8a-ad9c-e7d264641e58_TFG_Paola_Avila_Ebron.pdf (9.83M)

**Total de palabras:** 14049

**Total de caracteres:** 84792

# y3129424:TFG_Paola_Avila_Ebron.pdf

INFORME DE ORIGINALIDAD

| 13% | 6% | 9% | 6% |
|---|---|---|---|
| INDICE DE SIMILITUD | FUENTES DE INTERNET | PUBLICACIONES | TRABAJOS DEL ESTUDIANTE |

FUENTES PRIMARIAS

| | | |
|---|---|---|
| 1 | José Balsa-Barreiro, Dieter Fritsch. "Generation of visually aesthetic and detailed 3D models of historical cities by using laser scanning and digital photogrammetry", Digital Applications in Archaeology and Cultural Heritage, 2018<br>Publicación | 2% |
| 2 | classes.engr.oregonstate.edu<br>Fuente de Internet | 1% |
| 3 | spatialtechnologies.ca<br>Fuente de Internet | 1% |
| 4 | www.leica-geosystems.com<br>Fuente de Internet | 1% |
| 5 | Marine Fau, Raphaël Cornette, Alexandra Houssaye. "Photogrammetry for 3D digitizing bones of mounted skeletons: Potential and limits", Comptes Rendus Palevol, 2016<br>Publicación | 1% |
| 6 | aerial-photoco.uk<br>Fuente de Internet | 1% |

| | | |
|---|---|---|
| 7 | Thomas Luhmann, Stuart Robson, Stephen Kyle, Jan Boehm. "1 Introduction", Walter de Gruyter GmbH, 2013<br>Publicación | <1% |
| 8 | Submitted to The Hong Kong Polytechnic University<br>Trabajo del estudiante | <1% |
| 9 | Westoby, M.J., J. Brasington, N.F. Glasser, M.J. Hambrey, and J.M. Reynolds. "â€˜Structure-from-Motionâ€™ photogrammetry: A low-cost, effective tool for geoscience applications", Geomorphology, 2012.<br>Publicación | <1% |
| 10 | survey-odu.engr.odu.edu<br>Fuente de Internet | <1% |
| 11 | Submitted to University of Southampton<br>Trabajo del estudiante | <1% |
| 12 | www.int-arch-photogramm-remote-sens-spatial-inf-sci.net<br>Fuente de Internet | <1% |
| 13 | "Digital Heritage. Progress in Cultural Heritage: Documentation, Preservation, and Protection", Springer Science and Business Media LLC, 2016<br>Publicación | <1% |
| 14 | K. Wenzel, M. Rothermel, D. Fritsch, N. Haala. | |

| | | |
|---|---|---|
| | "IMAGE ACQUISITION AND MODEL SELECTION FOR MULTI-VIEW STEREO", ISPRS - International Archives of the Photogrammetry, Remote Sensing and Spatial Information Sciences, 2013<br>Publicación | <1% |
| 15 | Submitted to University of Cape Town<br>Trabajo del estudiante | <1% |
| 16 | Hengjian Tong, Yun Zhang, Zhenfeng Shao. "3D Remote sensing images online refining", 2009 17th International Conference on Geoinformatics, 2009<br>Publicación | <1% |
| 17 | www.tandfonline.com<br>Fuente de Internet | <1% |
| 18 | Submitted to The University of Manchester<br>Trabajo del estudiante | <1% |
| 19 | prezi.com<br>Fuente de Internet | <1% |
| 20 | Submitted to Birkbeck College<br>Trabajo del estudiante | <1% |
| 21 | Stephan Schreiber, Klaus G. Hinzen, Claus Fleischer, Sven Schütte. "Excavation-parallel laser scanning of a medieval cesspit in the archaeological zone cologne, germany", Journal on Computing and Cultural Heritage, 2012 | <1% |

| | | |
|---|---|---|
| | Publicación | |
| 22 | Submitted to University of Leeds<br>Trabajo del estudiante | <1% |
| 23 | cameradecision.com<br>Fuente de Internet | <1% |
| 24 | mdpi.com<br>Fuente de Internet | <1% |
| 25 | Submitted to University of Newcastle upon Tyne<br>Trabajo del estudiante | <1% |
| 26 | Submitted to Università degli Studi di Trieste<br>Trabajo del estudiante | <1% |
| 27 | www.mapindia.org<br>Fuente de Internet | <1% |
| 28 | Lecture Notes in Computer Science, 2012.<br>Publicación | <1% |
| 29 | Submitted to Polytechnic of Turin<br>Trabajo del estudiante | <1% |
| 30 | Heipke, Christian, Marguerite Madden, Zhilin Li, and Ian Dowman. "Theme issue “State-of-the-art in photogrammetry, remote sensing and spatial information science”", ISPRS Journal of Photogrammetry and Remote Sensing, 2016.<br>Publicación | <1% |
| 31 | Arnadi Murtiyoso, Pierre Grussenmeyer. | <1% |

| | | |
|---|---|---|
| | "Documentation of heritage buildings using close-range UAV images: dense matching issues, comparison and case studies", The Photogrammetric Record, 2017<br>Publicación | |
| 32 | Submitted to University of Bahrain<br>Trabajo del estudiante | <1% |
| 33 | Submitted to University of Pretoria<br>Trabajo del estudiante | <1% |
| 34 | www.freepatentsonline.com<br>Fuente de Internet | <1% |
| 35 | Submitted to Arizona State University<br>Trabajo del estudiante | <1% |
| 36 | Submitted to University of Plymouth<br>Trabajo del estudiante | <1% |
| 37 | Submitted to Pennsylvania State System of Higher Education<br>Trabajo del estudiante | <1% |
| 38 | Ruisheng Wang, Bisheng Yang, Florent Lafarge, Suya You. "Forward to the theme issue on point cloud processing", ISPRS Journal of Photogrammetry and Remote Sensing, 2018<br>Publicación | <1% |
| 39 | agile-online.org<br>Fuente de Internet | <1% |

| | | |
|---|---|---|
| 40 | S.N. Lane, K.S. Richards, J.H. Chandler. "Developments in photogrammetry; the geomorphological potential", Progress in Physical Geography, 2016<br>Publicación | <1% |
| 41 | Submitted to University of New South Wales<br>Trabajo del estudiante | <1% |
| 42 | Lerma, J.L.. "Terrestrial laser scanning and close range photogrammetry for 3D archaeological documentation: the Upper Palaeolithic Cave of Parpallo as a case study", Journal of Archaeological Science, 201003<br>Publicación | <1% |
| 43 | www.econstor.eu<br>Fuente de Internet | <1% |
| 44 | datatracker.ietf.org<br>Fuente de Internet | <1% |
| 45 | smudgemyart.com<br>Fuente de Internet | <1% |
| 46 | Submitted to University of Birmingham<br>Trabajo del estudiante | <1% |
| 47 | "Heritage and Archaeology in the DigitalAge", Springer Nature, 2017<br>Publicación | <1% |
| 48 | F. Tsai, H.-C. Lin. "Polygon-based texture | |

| | | |
|---|---|---|
| | mapping for cyber city 3D building models", International Journal of Geographical Information Science, 2007<br>Publicación | <1% |
| 49 | www.slideshare.net<br>Fuente de Internet | <1% |
| 50 | paudelnabin.blogspot.com<br>Fuente de Internet | <1% |
| 51 | Submitted to Universiti Teknologi Malaysia<br>Trabajo del estudiante | <1% |
| 52 | ericcolburn.com<br>Fuente de Internet | <1% |
| 53 | Brunier, Guillaume, Jules Fleury, Edward J. Anthony, Antoine Gardel, and Philippe Dussouillez. "Close-range airborne Structure-from-Motion Photogrammetry for high-resolution beach morphometric surveys: Examples from an embayed rotating beach", Geomorphology, 2016.<br>Publicación | <1% |
| 54 | Bashar Alsadik. "Practicing the geometric designation of sensor networks using the Crowdsource 3D models of cultural heritage objects", Journal of Cultural Heritage, 2018<br>Publicación | <1% |
| 55 | www.usbr.gov | |

| | | |
|---|---|---|
| | Fuente de Internet | <1% |
| 56 | Tae-Hyun Hwang, In-Hak Joo, Kyoung-Ho Choi. "An indexing method for spatial object in video using image processing and photogrammetry", IEEE International IEEE International IEEE International Geoscience and Remote Sensing Symposium, 2004. IGARSS '04. Proceedings. 2004, 2004<br>Publicación | <1% |
| 57 | "Full issue in PDF / Numéro complet en form PDF", GEOMATICA, 2011<br>Publicación | <1% |
| 58 | tel.archives-ouvertes.fr<br>Fuente de Internet | <1% |
| 59 | www.iirs.gov.in<br>Fuente de Internet | <1% |
| 60 | Submitted to University of Central England in Birmingham<br>Trabajo del estudiante | <1% |
| 61 | Submitted to University of Southern Queensland<br>Trabajo del estudiante | <1% |
| 62 | Submitted to University of Melbourne<br>Trabajo del estudiante | <1% |
| 63 | DeWitte, Debra J., Larmann, Ralph M., Shields, | |

| | | |
|---|---|---|
| | M. Kathryn. "Gateways to Art (Third Edition)", Thames & Hudson<br>Publicación | <1% |
| 64 | Surya S.C. Congress, Anand J. Puppala, Cody L. Lundberg. "Total system error analysis of UAV-CRP technology for monitoring transportation infrastructure assets", Engineering Geology, 2018<br>Publicación | <1% |
| 65 | Submitted to DISC Royal School of Military Survey<br>Trabajo del estudiante | <1% |
| 66 | Submitted to Leiden University<br>Trabajo del estudiante | <1% |

| | | | |
|---|---|---|---|
| Excluir citas | Activo | Excluir coincidencias | < 5 words |
| Excluir bibliografía | Activo | | |